DEVELOPMENT OF BORIDES/BORATES FOR ENERGY STORAGE DEVICES

A THESIS SUBMITTED TO
THE GRADUATE SCHOOL OF NATURAL AND APPLIED SCIENCES
OF
MIDDLE EAST TECHNICAL UNIVERSITY

BY

DORUK BAHTİYAR

IN PARTIAL FULFILLMENT OF THE REQUIREMENTS
FOR
THE DEGREE OF MASTER OF SCIENCE
IN
METALLURGICAL AND MATERIALS ENGINEERING

SEPTEMBER 2022

Approval of the thesis:

DEVELOPMENT OF BORIDES/BORATES FOR ENERGY STORAGE DEVICES

submitted by **Doruk BAHTİYAR** in partial fulfillment of the requirements for the degree of **Master of Science** i**n Metallurgical and Materials Engineering, Middle East Technical University** by,

Prof. Dr. Halil Kalıpçılar
Dean, Graduate School of **Natural and Applied Sciences** _____

Prof. Dr. Ali Kalkanlı
Head of the Department, **Metallurgical and Materials Eng., METU** _____

Prof. Dr. M. Kadri Aydınol
Supervisor, **Metallurgical and Materials Eng., METU** _____

Examining Committee Members:

Prof. Dr. Emren Nalbant
Chemistry, METU _____

Prof. Dr. M. Kadri Aydınol
Metallurgical and Materials Eng., METU _____

Prof. Dr. Zafer Evis
Engineering Sciences, METU _____

Assoc. Prof. Dr. Burak Ülgüt
Chemsitry, Bilkent University _____

Assoc. Prof. Dr. Harun Koku
Chemical Eng., METU _____

Date: 01.09.2022

I hereby declare that all information in this document has been obtained and presented in accordance with academic rules and ethical conduct. I also declare that, as required by these rules and conduct, I have fully cited and referenced all material and results that are not original to this work.

Name Last name : Doruk Bahtiyar

Signature :

ABSTRACT

DEVELOPMENT OF BORIDES/BORATES FOR ENERGY STORAGE DEVICES

Bahtiyar, Doruk
Master of Science, Metallurgical and Materials Engineering
Supervisor : Prof. Dr. M. Kadri Aydınol

September 2022, 67 pages

For many years, materials in the form of metal sulfides, oxides, phosphates, and titanates have been developed as cathode and anode active materials to be used in energy storage devices. Borides and borates, recently, attracted the attention of researchers in this field. In this study, for the development of a new class of materials for energy storage applications, synthesis and characterization of metal (Fe, Mo, Mn, and V) borides and (Mn, and Y)borates were carried out. The obtained materials were tested for their activity in lithium-ion batteries. Chemical and structural analysis were performed using X-ray diffraction spectroscopy, and scanning electron microscopy. Electrochemical characterization of the cells showed that manganase boride has the highest initial specific capacity of 576.80 mAh/g while yittrium borate has a specific capacity of 78.54 mAh/g as lowest at 20 mA/g current density. After fifty cycles at 20 mA/g, capacity decrease was observed for all samples, capacity retention of VB was calculated as 85.37 % which was the highest among all samples that are synthesized during this study. Furthermore, cyclic voltammetry was applied to understand charge-discharge mechanism of samples. It was noted that all samples has SE_1 formation around 0.74 V.

Keywords: Boride, borate, Li-ion battery, solid-state reaction synthesis

ÖZ

BORÜR VE BORATLARIN ENERJİ DEPOLAMA SİSTEMLERİ İÇİN GELİŞTİRİLMESİ

Bahtiyar, Doruk
Yüksek Lisans, Metalurji ve Malzeme Mühendisliği
Tez Yöneticisi: Prof. Dr. M. Kadri Aydınol

Eylül 2022, 67 sayfa

Metal sülfat, oksit, fosfat ve titanat formunda malzemelerin enerji depolama sistemlerinde anotta ve katotta aktif malzeme olarak kullanılması üzerine çalışmalar yıllardır yapılmaya devam ediyor. Son dönemde borür ve boratlar da bu konuda araştırma yapanların dikkatini çekti. Bu çalışmada yeni bir malzeme sınıfının enerji depolama uygulamalarında kullanılmak üzere geliştirilmesi için metal (Fe, Co, Mn, ve V) borür ve (Mn ve Y) boratlarının sentezi ile karakterizasyonu yapıldı. Elde edilen malzemeler aktivitelerini anlamak için lityum iyonda test edildi. Malzemelerin kimyasal ve yapısal analizleri x-ışınları kırınım spektroskobu ve tarayıcı elektron mikroskobu ile yapıldı. Hücrelerin elektrokimyasal karakterizasyonu 20 mA/g akım yoğunluğunda mangan borürün 576.80 mAh/g ile en yüksek ilk desarj spesifik kapasitesine, itriyum boratın ise en düşük olan 78.54 mAh/g spesifik kapasitesine sahip olduğunu göstermiştir. Tüm numunede 20 mA/g akım yoğunluğunda yapılan elli çevrimden sonra kapasite düşüşü gözlenmiştir ve arasında en yüksek kapasite korunumunun % 85.37 ile vanadyum borüre ait olduğu hesaplanmıştır. Ek olarak numunelere döngüşümlü voltametri uygulanmış ve tüm örneklerin 0.74 V civarında katı elektrolit arayüzü oluşturduğu gözlendi.

Anahtar Kelimeler: Borür, borat, Li-iyon batarya, katı hal reaksiyon sentezi

Dedication to

My family

ACKNOWLEDGMENTS

First, I would like to thank my advisor, Prof. Dr. M. Kadri AYDINOL for his encouragement, patience, sharing his knowledge and endless support. His attitude and knowledge were played great role at my self-improvement throughout this study.

I want to thank Cansu Savaş Uygur and Kadir Özgün Köse for their support, help, guidance, encourgament and sharing their knowledge continuously throughout my research. I also thank Mustafa Alp Yıldırım for his friendship and help.

I want to thank Naz Baysal, Sevgi Ekin Bayram, Melih Ögeday Çicek and İsmail Eken for their endless friendship and mental support during this study.

I want to thank more than anyone to my parents Raci and Okşan Bahtiyar for making me who I am and their support, love anytime I needed. I am so thankful to have them as my parents.

TABLE OF CONTENTS

LIST OF TABLES

TABLES

LIST OF FIGURES

FIGURES

LIST OF ABBREVIATIONS

SHE	Standard Hydrogen Evolotion
LCO	Lithium Cobalt Oxide
LFP	Lithium Iron Phosphate
LNO	Lithium Nickel Oxide
NCA	Lithium Nickel Cobalt Aluminium Oxide
rGO	Reduced Graphene Oxide
SEI	Solid Electrolyte Interface
CV	Cyclic Voltammetry
XRD	X-ray Diffraction

CHAPTER 1

INTRODUCTION

1.1 Development of Secondary Lithium-ion Batteries

Usage areas of electricity and the number of electronic devices have hugely grown over the last half-century. The growth of the electronic industry created a problem which is the performance of secondary batteries that are already used in these devices. Abilities and processes that a portable device can do enhanced over time that led to a need for higher energy density batteries since these processes require more energy.

Lead-acid and nickel metal hydride batteries have been used for several years in the industry as batteries for portable devices or vehicles. A metal that has a very high reduction voltage (-3.04 V vs SHE) attracted the attention of researchers[1]. Lithium not only serves excellent reduction potential but also has a good diffusion coefficient as one of the smallest elements that makes it a great candidate to be used as battery material at high power demanding electronic device batteries[2]. Over several years, lithium has been used and developed as electroactive material in batteries with different chemistries.

Lithium cobalt oxide (LCO) cathode batteries are one of the commercialized batteries that is developed throughout research on lithium-based battery chemistries. It has a layered Lithium Cobalt Oxide as a cathode with a graphite anode. With its layered oxide structure that can be seen in Figure 1.1, Cobalt Oxide is a great host and provides an easy path for lithium atoms to go in and out during lithiated and delithiated states of the battery. LCO has a high specific capacity (274 mAh/g) with good cyclability and high discharge voltage[3] which makes it one of the most used

batteries currently for portable electronic devices. Despite its excellent properties, there are also several problems with LCO. First of all, the cost is a huge issue for this battery chemistry due to cobalt which is an expensive metal. Moreover, it has a significantly low thermal runaway temperature (150 °C) with huge capacity decay at abused conditions since voltages above 4.3 V phase change occur at the cathode of the battery. Both of these problems create safety risks during the usage of LCO batteries.

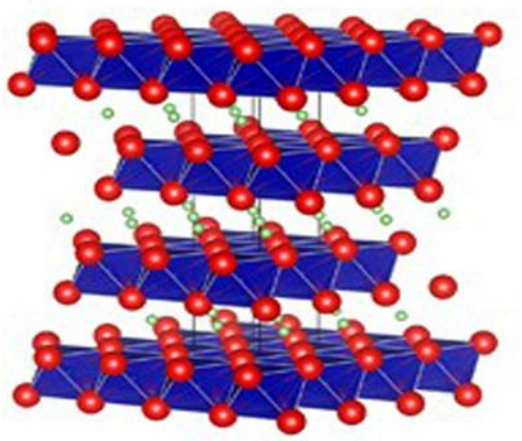

Figure 1.1. Crystal structure of Lithium Cobalt Oxide[4]

Materials with olivine structure (Figure 1.2.) were discovered in the same decade as layered oxides. Goodenough with his research group introduced a differently structured cathode material than LCO which is Lithium iron phosphate[5]. Graphite anode with $LiFePO_4$ cathode provides excellent cycle life with better structural stability at higher voltages than LCO. Moreover, the abundance of iron results in a significant decrease in battery cost. Regardless of its cost and cyclic stability, one of the main problems that LFP batteries had is their usage temperature is limited to positive degrees since their capacity decays seriously at temperatures below 0 °C[6]. Moreover, the electrical conductivity of the phosphate group is another important drawback of LFP batteries. This problem has been tried to overcome with a carbon coating, dopants, and additives.

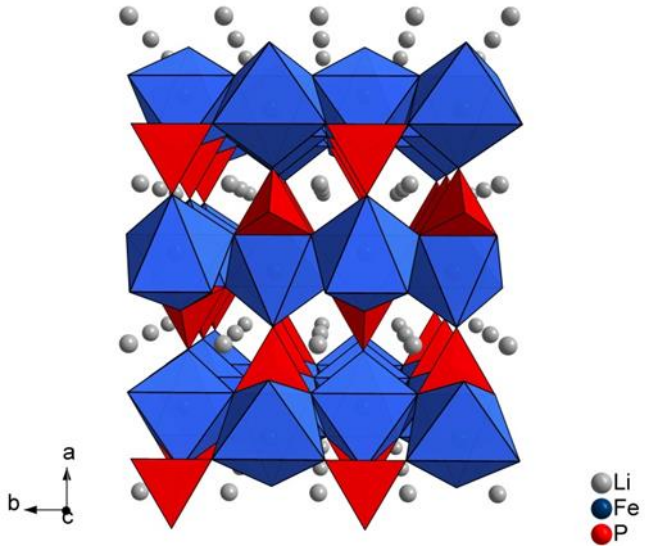

Figure 1.2. Lithium iron phosphate crystal structure[7]

The cost of the battery is an important parameter that researchers must consider during the production of newly founded lithium chemistries. Lithium nickel oxide cathode material (LNO) was proposed and investigated as alternative chemistry to LCO. Despite its high theoretical capacity (275 mAh/g) with nickel being lower cost than cobalt, the synthesis of lithium nickel oxide results in a non-stoichiometric oxide[8]. The ionic radius of nickel and lithium are close enough so nickel ions can be placed at lithium sites in the crystal structure.

The problems mentioned are solved by doping LNO with cobalt and aluminium. Cobalt as dopant not only increases the stability of structure but also decreases the number of nickel ions occupying lithium sites[9]. Aluminium does not have any electrochemical activity in battery, it improves the stability of chemistry at elevated temperatures as a consequence of atmospheric conditions or heat created by the cell itself. NCA batteries show a higher specific capacity (200 mAh/g) with longer calendar life than conventional layered oxide batteries. Not only aluminium but also manganese is used to improve stability of lithium nickel cobalt structure. Lithium nickel manganese cobalt which is one of the widely studied cathode chemistry

alongside NCA. Although $LiNi_1Mn_1Co_1O_2$ delivers lower specific capacity (160 mAh/g) than NCA, it has good rate capability[10]. Various compositions of NMC compound are studied throughout years, effect of composition on stability and specific discharge capacity of battery can be seen at Figure 1.3.

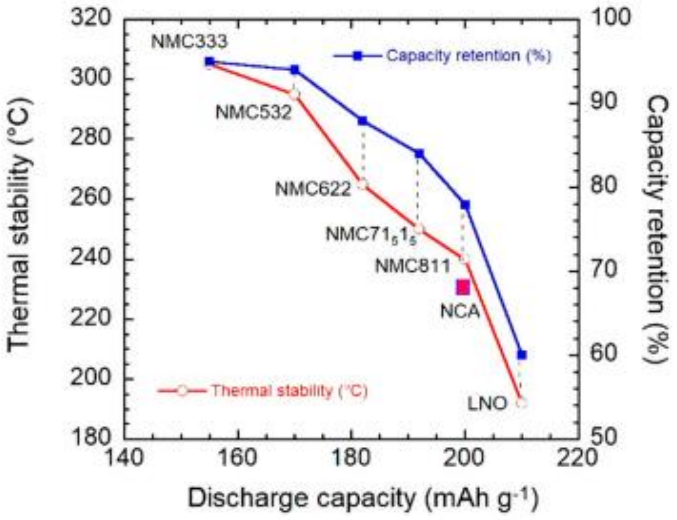

Figure 1.3. Thermal stability and specific capacity of various NMC compositions[11]

Notable changes in cell chemistries with foundation of new battery materials are accepted as new step at cell generation. Second generation of cells had been started with NMC in Figure 1.4. At third generation, improvement of cathode materials was followed by addition of silicon to graphite anodes to enhance their properties. Although, graphite stands as a great anode material with good cycle life, low cost and excellent cyclic efficiency, addition of small percentage of Si leads a better electrically conductive anode. As a result, higher specific capacity anode for lithium ion batteries could achieved[12]. Searching for new anode materials to get one step further at cell generation continued throughout years. Boron based materials get in to interest of researchers because of that reason.

Cell Generation	Cell Chemistry
Generation 5	• Li/O2 (lithium-air)
Generation 4	• All solid-state + lithium anode • Conversion materials (primarily lithium-sulphur)
Generation 3b	• Cathode: HE-NMC, HVS (high-voltage spinel) • Anode: silicon/carbon
Generation 3a	• Cathode: NMC622 to NMC811 • Anode: carbon + silicon (5 to 10%)
Generation 2b	• Cathode: NMC523 to NMC622 • Anode: carbon
Generation 2a	• Cathode: NCM111 • Anode: 100% carbon
Generation 1	• Cathode: LFP, NCA • Anode: 100% carbon

Figure 1.4. Generation of cells[13]

1.2 Scope of Thesis

Foundation of new cell generations throughout years leads us to the usage and development of different materials as active materials in lithium-ion batteries is an ongoing process. Researchers showed that boron-based materials have good electrochemical activity as electroactive species which leads them to investigate their properties inside battery chemistry. Experiments measurements and computational calculations showed that the specific capacity and reversibility of boron-based materials are high enough to replace commonly used materials. In the published literature, there is a lack of information on electrochemical tests of borides and borates. In most cases, computational methods were not supported with hands-on experiments, and most common battery material compositions which include Co, Fe, Ni, etc. were not tested as metal boride or borate.

In this study, manganese, iron, molybdenum, vanadium borides, and manganese, yttrium borate were synthesized with different routes and investigated as future anode active material at Li-ion batteries.

CHAPTER 2

LITERATURE REVIEW

2.1 Metal Borides and Borates at Lithium-Ion Battery

In the last two decades, borides and borates investigated in lithium batteries as both anode and cathode to see if they are suitable for application areas. As cathode materials commonly $LiFePO_4$ is accepted as the best candidate for mass production due to its cost, chemical performance, and stable usage[14–17]. Since borates show the stability of the polyanion group as phosphates do against oxygen loss, they are examined as cathode material in lithium-ion batteries.

2.1.1 Boron-based Materials as Cathodes

As mentioned above, lithium metal borates are introduced to literature as a stable polyanion group that could replace LFP cathode. Yamada et al.[18] introduced $LiFeBO_3$ as a better alternative than LFP cathode. They calculated via ab initio that a theoretical capacity of 220 mAh/g could be achieved with iron borate cathode active material. Electrochemical experiments were made to support their calculated data and a specific capacity of 200 mAh/g was achieved over 20 cycles at a 0.05C rate with a noticeably smaller volume expansion than other known intercalation cathodes. Despite its high capacity, there were also two main problems with the usage of $LiFeBO_3$ as cathode material. The voltage window was too large for practical applications and powders suffers high moisture sensitivity.

$LiMnBO_3$ was examined computationally and electrochemically by researchers. Zhang et al.[19] synthesized bare $LiMnBO_3$ with carbon encapsulated composite of the

same material to study its specific capacity and capacity retention. Composite was mainly done to overcome major drawbacks which were previously seen at $LiFeBO_3$. Bare $LiMnBO_3$ showed 110 mAh/g specific capacity over 50 cycles at 0.05C rate which drops significantly with an increase at C-rate. Carbon encapsulated borates have been shown better performances than bare borate. Specific capacity of 150 mAh/g achieved over same cycle number at stated C-rate. However, capacity drop during higher C-rates cannot be solved as intended. Afyon et al. [20] approached $LiMnBO_3$ cathode from a different perspective. They examined the effect of particle size with also reduced Graphene Oxide (rGO) coating on specific capacity and rate capability of manganese borate as cathode active material. A significant capacity drop was seen for both hexagonal and monoclinic $LiMnBO_3$ which are sub-micron in size after second discharges. A specific capacity of 38 mAh/g was achieved after the second cycle of m-$LiMnBO_3$ while hexagonal borate also shows 49 mAh/g. A decrease in particle size increased the specific capacity of material remarkably while reducing the capacity drop in the second cycle. Nano size hexagonal $LiMnBO_3$ was shown 140 mAh/g specific capacity during first discharge and its capacity dropped only 20 mAh/g after secondary discharge of the cell. As the study continues, not only particle size but also rGO coating improved the properties of metal borate notably. rGO coated $LiMnBO_3$ was shown a specific capacity of 120 mAh/g over 10 cycles at 0.05C and the capacity drop with an increase in C-rates was remarkably less than the borates mentioned previously. Moreover, Kim et al.[21] observed that a decrease in particle size also improves the electrochemical properties of monoclinic $LiMnBO_3$. They claimed that the specific capacity and rate capability of m-$LiMnBO_3$ could be increased by the addition of Fe with substitutional Mg. Results show that $LiMnFeMgBO_3$ cathode can achieve a near theoretical capacity of 200 mAh/g at 0.02C which is also supported with ab inito calculations. This specific borate possesses significantly better rate capability than other borates that were examined in the literature. A specific capacity of 175 mAh/g was measured at 0.05C and it dropped to 120 mAh/g at 1C. This result indicates that not only particle size but also

the addition of other metals improves the electrochemical properties of lithium metal borates as cathode active materials.

A brief electrochemical property summary of the research mentioned above can be seen at following Table 2.1.

Table 2.1 Electrochemical Properties of Lithium Metal Borates as Li-ion Cathode

Metal Borate	*Conductive Additive*	*Specific Capacity at 0.05C (mAh/g)*		*Specific Capacity at 1C (mAh/g)*
		1st Cycle	*2nd Cycle*	
$LiFeBO_3$[18]	-	200	190	160
$LiMnBO_3$[19]	-	160	160	40
$LiMnBO_3$[19]	carbon	150	150	60
Nano h-$LiMnBO_3$[20]	-	140	120	-
Nano h-$LiMnBO_3$[20]	rGO	145	140	-
$LiMnFeMgBO_3$[21]	carbon	180	175	120

2.1.2 Boron-based Materials as Anodes

Graphite is the material that currently dominates the commercialized anode active material in the industry. It has a theoretical specific capacity of 372 mAh/g with a 0.05 V lithium insertion potential[22]. Search for new materials to replace graphite continued through the last two decades. Improving capacity was the main goal of this research. Not only capacity but also one of the drawback which is low intercalation voltage has been tried to overcome. That low potential could result in a lithium dendrite formation which results in catastrophic failure of the battery.

2.1.2.1 Borates

Borates are taken into the interests of researchers throughout the search for new materials as anode active species in Li-ion batteries. The bond between boron and oxygen atom has a relatively small induction, which results in a higher lithium reduction potential than commercial graphite.

At earlier 2000s Ibarra-Palos et al.[23] conducted their research on two different iron borates. Their experiments were shown that both $FeBO_3$ and Fe_3BO_6 have higher redox potential than graphite. Discharge plateaus were observed at 1.20 V and 1.42 V, respectively. After the first discharge cycle, the redox potential of $FeBO_3$ raised to over 1.50 V. The initial discharge plateau of this borate is significantly longer than Fe_3BO_6 which is the result of a two-phase reaction for both borates. The effect of these reactions can be seen in the reversible capacities of borates. At initial discharges, specific capacities of $FeBO_3$ and Fe_3BO_6 were obtained as 750 mAh/g and 860 mAh/g at 0.05C, respectively. Around the 10^{th} cycle, capacity for both borates came to 250 mAh/g and the capacity drop rate was decreased. Even if large capacity drops were observed, obtained capacity for $FeBO_3$ and Fe_3BO_6 were higher than capacities for most cathode active materials that are commercially used. Moreover, lithium reduction reaction potentials are significantly lower than graphite. Work on iron-based borate was continued more.

Yu et al.[24], synthesized hollow porous amorphous iron borate particles to investigate their properties as Li-ion battery anode. They aimed to synthesize hollow spherical nanoparticles to improve the diffusivity of lithium so that reaction kinetics for lithiation and delithiation become faster. Like previous work, an irreversible phase change occurs for hollowed porous FeBO. That irreversible reaction is referred to as solid electrolyte interface (SEI) formation. Formed SEI covers the active surface of the material as well as causes a decomposition of the electrolyte. The initial discharge capacity of HP-FeBO is 1600 mAh/g at 100mA/g current density. After the first cycle capacity drops to 1000 mAh/g which is significantly higher than previously mentioned iron borates and commercial graphite. Moreover, after 25 cycles capacity

decay disappears and specific capacity increases to initial discharge capacity then maintains its stability for 300 cycles. HP-FeBO has shown remarkable specific capacity with excellent rate capability, and voltage plateau for lithium redox reaction is observed around 1.0 V which is also better than graphite.

Zeng et al.[25] researched vanadium borate and investigated its electrochemical properties. The experiment took place for V_3BO_6. As mentioned above like iron borate, vanadium borate also suffers from capacity decay after the initial discharge cycle. It is pointed out that irreversible plateau for two-phase reaction occurred at the same voltage with iron borates. At first discharge, bare V_3BO_6 has a specific capacity of 1000 mAh/g at 10 mA/g current density, and capacity drops to 600 mAh/g in the second cycle. Capacity drop decreased after several cycles and a stable capacity of 410 mAh/g was achieved after 50 cycles.

Another vanadium borate which is VBO_3 also examined as possible anode material for lithium batteries. Kim et al.[26] synthesized and explained its electrochemical properties. The first discharge cycle of VBO_3 showed that two different irreversible reactions occur for this borate. Firstly, previously mentioned SEI formation occurs during the cyclic process after that another reaction which is the transformation of structure from crystalline vanadium borate to amorphous were taken place. A specific capacity of 560 mAh/g at 0.2 mA/cm^2 was observed after initial discharge, capacity decreased after certain cycles and 360 mAh/g was measured after 50 cycles. For both vanadium borates, even if capacity decay is observed, their capacities are much higher than currently used anode materials at Li-ion battery chemistries. As mentioned before, carbon coating was made for cathode active borates, and improvement in electrochemical properties has been seen. The coating was applied on vanadium borate as well to improve its cyclic performance and hinder capacity drop throughout cycles.

Wu et al.[27], managed to synthesize carbon coated, and crystalline VBO_3. A specific capacity of 1200 mAh/g was measured for the initial discharge of VBO_3-c and capacity dropped to 900 mAh/g after the second cycle at 20 mA/g current density.

Despite the decrease in capacity observed after the second cycle, its decrease is relatively less than previously recorded studies. However, carbon coating did not improve the rate capability of VBO_3.

A summary of electrochemical results of metal borates as anode active material in the lithium-ion battery is represented in the following Table 2.2.

Table 2.2 Electrochemical Properties of Metal Borates as Li-ion Anode

Borate	*Reference*	*Initial Discharge Capacity (mAh/g) (Current density)*	*Overall Specific Capacity(mAh/g) (Current density)*
$FeBO_3$	[23]	750 (0.05 C)	250 (0.05 C)
Fe_3BO_6	[23]	860 (0.05 C)	250 (0.05 C)
HP-FeBO	[24]	1600 (100 mA/g)	1600 (100 mA/g)
V_3BO_6	[25]	1000 (10 mA/g)	410 (10 mA/g)
VBO_3	[26]	560 (0.2 mA/cm^2)	360 (0.2 mA/cm^2)
VBO_3-c	[27]	1200 (20 mA/g)	900 (20 mA/g)

2.1.2.2 Borides

Research on boron-based material as anode active material in lithium-ion batteries is not limited to borates, borides have also been investigated. A boron atom can react with five lithium atoms which gives one of the highest theoretical capacities could achieve which is 12395 mAh/g[28]. Even if having a high theoretical capacity, metal boride literature about being Li-ion anode active materials was limited. Furthermore, the synthesis of borides is a challenging process that requires high-temperature or

high-pressure methods. In the last decade, computational works have been conducted that convinced researchers to work on metal borides experimentally.

Guo et al.[29], came at 2D metal borides possibility as anode material at Li-ion battery. 2D MXene-like borides are possible to synthesize and they could be suitable materials to replace graphite in commercial batteries. The research was made computationally to calculate the properties of Mo_2B_2 and Fe_2B_2. With the help of computational methods diffusion energy barriers for lithium, and atom insertion were calculated for different diffusion paths. It is claimed that diffusion energy barriers for both molybdenum and iron boride are lower than for graphite. Moreover, the theoretical specific capacities of Mo_2B_2 and Fe_2B_2 were calculated as 440 mAh/g and 660 mAh/g, respectively.

Gao et al.[30], operated another computational research on two-dimensional metal boride which is yttrium boride. They mentioned that the diffusion energy barrier for lithium ions inside Y_2B_2 is comparable with other commercial anodes like graphite and Y_2B_2 possesses a theoretical capacity of 806 mAh/g which makes it a promising material as anode active material.

2D MXene like MoB was managed to synthesize and its electrochemical properties were investigated. Xiong et al.[31] synthesized pure two-dimensional MoB and measured its capacity as anode active material in Li-ion battery. A specific capacity of 700 mAh/g was observed after the initial discharge cycle at a 50 mA/g current rate. Capacity drop at the second cycle was remarkably low which is 50 mAh/g and the material showed a stable reversible capacity of 150 mAh/g over 1000 cycles at 2 A/g current density.

Netz et al.[32], conducted one of the earliest researches on different metal borides to report their suitability for Li-ion battery applications. The experimental procedure took place on B_4C, CaB_6, LaB_6, and SiB_3. Borides rather than silicon showed below 50 mAh/g initial discharge capacities which are not promising for anode applications. On the other hand, SiB_3 has a specific capacity of 920 mAh/g at initial

discharge. After the second discharge capacity drops to 440 mA/g which is relatively higher than graphite as well.

There are some experimental studies on various cobalt borides. Liu et al.[33], synthesized CoB, Co_2B, and Co_3B to measure their electrochemical properties. These borides showed the specific capacity of 190, 175, and 88 mAh/g at 25 mA/g current density, respectively. It could be claimed that a decrease in boron content inside metal boride causes a decrease in the specific capacity of the material. On the other hand, these borides do not show a capacity drop after initial discharge. Their capacity increases for several cycles where they are activated and stable capacity is obtained after these cycles.

Graphene anchored CoB was also studied by researchers. Wang et al.[34], anchored cobalt boride particles on graphene to improve its stability as anode active material. They claimed that bare CoB shows the specific capacity of 750 mAh/g at 50 mA/g current density, and it decreased to 250 mAh/g after 5 cycles. Reduced graphene oxide anchored CoB has an extremely higher initial discharge capacity which is 1400 mAh/g than bare boride and its capacity becomes stable after several cycles and shows 600 mAh/g. Moreover, they also experimented to explain the reasoning for capacity decay after the first cycle. Their experiment shows that at the initial discharge of battery below 0.8 V an irreversible reaction occurs. That reaction was related to the decomposition of electrolytes with the formation of the SEI layer. Similar phenomena were mentioned before at borates as well.

A summary of electrochemical results of metal borides as anode active material in the lithium-ion battery is represented in the following Table 2.3.

Table 2.3 Electrochemical Properties of Metal Borides as Li-ion Anode

Boride	*Reference*	*Theoretical Capacity(mAh/g) (Computationally calculated)*	*Initial Discharge Capacity (mAh/g) (Current density)*	*Overall Specific Capacity(mAh/g) (Current density)*
Mo_2B_2	[29]	440	-	-
Fe_2B_2	[29]	660	-	-
Y_2B_2	[30]	806	-	-
MoB	[31]	-	700 (mAh/g)	150 (2A/g)
SiB_3	[32]	-	920	440
CoB	[33]	-	170 (25mAh/g)	190 (25mAh/g)
Co_2B	[33]	-	120 (25mAh/g)	175 (25mAh/g)
Co_3B	[33]	-	40 (25mAh/g)	88 (25mAh/g)
CoB	[34]	-	750 (50mAh/g)	250 (50mAh/g)
GA-CoB	[34]	-	1400 (50mAh/g)	600 (50mAh/g)

CHAPTER 3

EXPERIMENTAL PROCEDURE

In this study, two different production approaches were applied to synthesize borides and borate of metals, solid state and precipitation synthesis routes. At the synthesis of materials sodium borohydride ($NaBH_4$)(Aldrich, 98.0 %), sodium hydroxide (NaOH)(Aldrich, 98.0 %), manganese chloride tetrahydrate ($MnCl_3$.4H2O)(Aldrich, 98.0 %, vanadium oxide (V_2O_3)(Aldrich, 98.0 %), molybdenum oxide (MoO_3) (Aldrich, 99.5 %) (Aldrich, 98.0 %), manganese oxide (MnO_2)(Aldrich, 90.0 %), iron oxide (Fe_2O_3) (Aldrich, 97.0 %) were used.

Solid state synthesis is one of the methods that is used in this study to produce borides easier and cheaper than other known methods specifically. Another production route is precipitation which is used to produce $Mn(BO)_3$.

3.1 Solid State Synthesis

During the study, borides are synthesized with this production method[35]. Metal oxide powders were mixed with boron source, which is Sodium Borohydride 1 to 4 molar ratio, respectively. The mixture is ball-milled for 3 hours at 100 rpm. After the milling, the powder mixture is poured into alumina or stainless-steel crucibles to be placed inside the atmosphere-controlled furnace. Powders were kept under 900 °C for 30 minutes under 1.5 L/min argon flow. Produced samples were ground by hand mortar and then washed with boiling water several times to get rid of any residual sodium-based material. Excess water was removed via vacuum filtering and powders were dried at 60 °C for 2 hours under vacuum.

3.2 Precipitation Synthesis

Manganese borate was synthesized with a different method than others as mentioned above[36]. Manganese chloride and $NaBH_4$ were dissolved in distilled water at different bakers with a 1:1.5 molar ratio, respectively. Beaker that contains chloride was placed in an ice bath to drop the solution temperature to 5 °C. When chloride solution was cooled enough, a solution of 7.5 wt.% $NaBH_4$ and 7.5 wt.% NaOH was added dropwise with a 3.5 ml/min drop rate. The solution was stirred continuously during and after the process and newly formed precipitates were collected, washed, and filtered. The powder was poured into an alumina crucible and placed in a furnace under an argon atmosphere where they were kept under 300 °C for 2 hours.

3.3 Physical Characterization

Borides and borate that were synthesized with previously mentioned procedures were analyzed with X-ray Difftactometry with Rigaku DMAX 2200 and Bruker at Metallurgy and Materials Engineering Department. Analysis occurred between various degrees with a 2°/min step size. Match software was used to fit obtained X-ray Diffraction patterns of MoB, MnB, FeB, VB, and $Mn(BO_3)$. Moreover, the morphology of samples was examined by using Scanning Electron Microscopy (FEI Nova Nano 430) with various images at different magnifications.

3.4 Electrochemical Characterization

For electrochemistry-related characterizations which are Cyclic Voltammetry, Galvanostatic Charge-Discharge, and Electrochemical Impedance Spectroscopy, were made at button cell configuration. Pure litium was used as a counter electrode. Experiments were made with Biologic MPG2 which is located at Metallurgy and Materials Engineering Department.

Electrodes for button cell configuration were prepared by the slurry method. All powders were mixed with vacuum dried carbon black and polyvinylidene difluoride with a 70:20:10 weight ratio, respectively. The slurry was stirred with a ball mill for 20 minutes at 15 Hz/min. By using Doctor Blade, the stirred slurry was coated on copper foil. Coated foil dried under vacuum for 2 hours at 120 °C, taken out to cut 18 mm discs then put under vacuum for overnight drying. Button cells were assembled inside a glove box. During assembly, a thick glass fiber separator,pure lithium coins, and 1M $LiPF_6$ which dissolved in 50:50 EC: DEC solution were used.

3.4.1 Galvanostatic Charge and Discharge

The produced cells were initially discharged at 20 mA/g current density and then cycled 4 times at that current between 0.02 and 3.00 V. The galvanostatic cycles continued with five cycles at 50 and 100 mA/g current density. To determine rate capability, cells were cycled 5 times again at 20 mA/g current density. Moreover, the cyclic stability of cells was tested with different button cells. Freshly configurated cells cycled over 50 times at 20 mA/g current density.

3.4.2 Cyclic Voltammetry

CV was applied on cells for three cycles at a scan rate of 0.02 mV/s and one more cycle at 0.05 and 0.08 mV/s scan rates. The potential range of CV was chosen the same with galvanostatic charge and discharge. The initial scan was made through the discharge of the cell. CV was made at two electrode configurations, reference electrode was not used.

CHAPTER 4

RESULTS AND DISCUSSION

4.1 Physical Characterization

The temperature was a key parameter to synthesize impurity-free borides throughout this study. Ball milling is not considered an important parameter since it is applied for the homogeneous mixing of particles. As mentioned by Zoli et al.[37] with an increase in temperature amount of sodium-based impurities is decreased. As can be seen in Figure 4.1, vanadium boride synthesis was made at 500, 700, and 900 °C to declare the optimum synthesis temperature for sodium-based material-free borides. At 500 °C, the temperature was not enough for a solid-state reaction to occur. $NaBH_4$ does not go under reaction with V_2O_3 as a result bare vanadium oxide remained as it is. An increase in temperature resulted in a reaction of powders, and sodium metaborate ($NaBO_2$) was formed. At 900 °C reaction (1) similar to:

$$MO + 3NaBH_4 \Rightarrow MB_2 + 2Na(l,g) + NaBO + 6H_2 \qquad (1)$$

occurred completely. Na and H were evaporated at a given temperature and the remaining sodium-based materials were washed. Synthesis of orthorhombic VB was achieved at 900 °C via solid state production method.

This temperature was accepted as the main production temperature for borides and all borides are synthesized at that temperature. Synthesis of vanadium, iron, molybdenum, manganese boride and yttrium borate were achieved at a given temperature. MnB is the only sample that has multiple phases in it, MnB_2 and MnB_4 phase mixture was observed after synthesis (Figure 4.2). Molybdenum diboride (Figure 4.3), iron boride (Figure 4.4), and vanadium boride (Figure 4.5) were borides that managed to be synthesized throughout this study and their XRD graphs are plotted as follows.

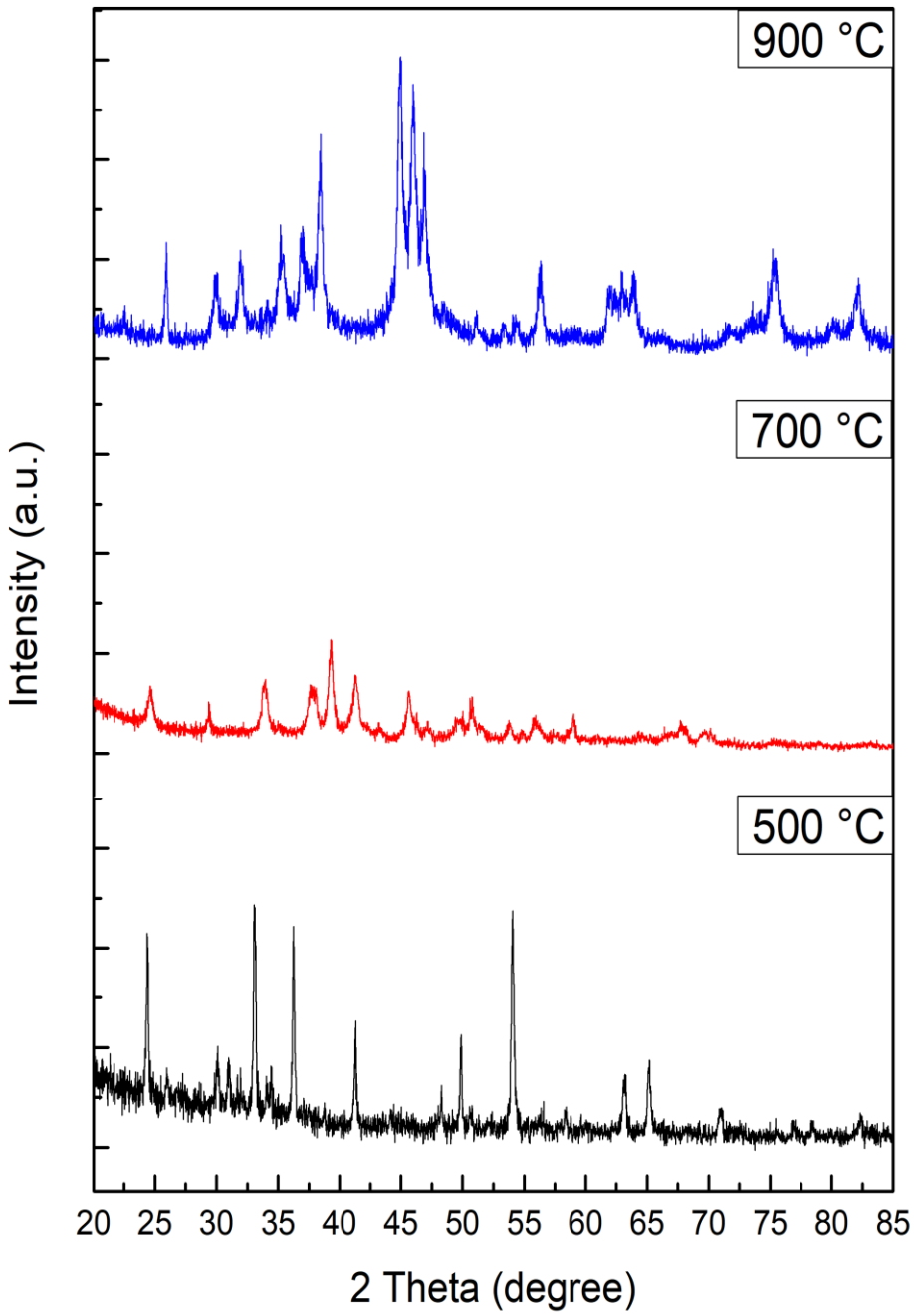

Figure 4.1. XRD patterns of V_2O_3-$NaBH_4$ mixture after synthesis at 500 - 900 °C.

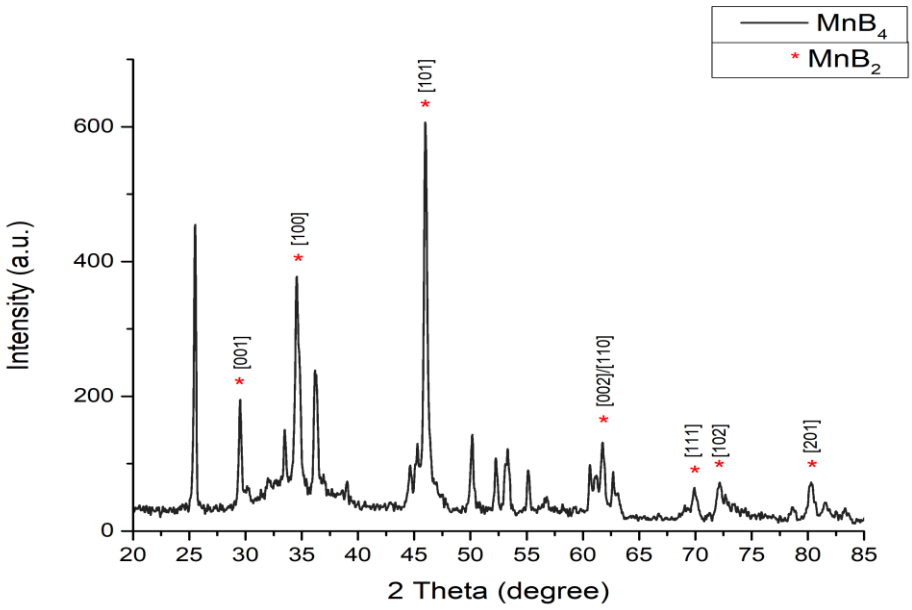

Figure 4.2. XRD pattern of MnB.

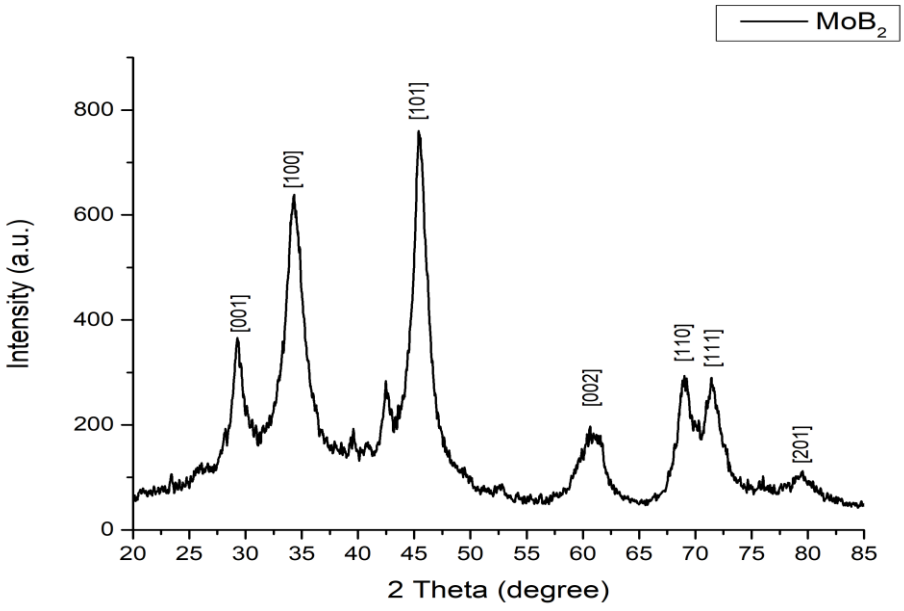

Figure 4.3. XRD pattern of Mo

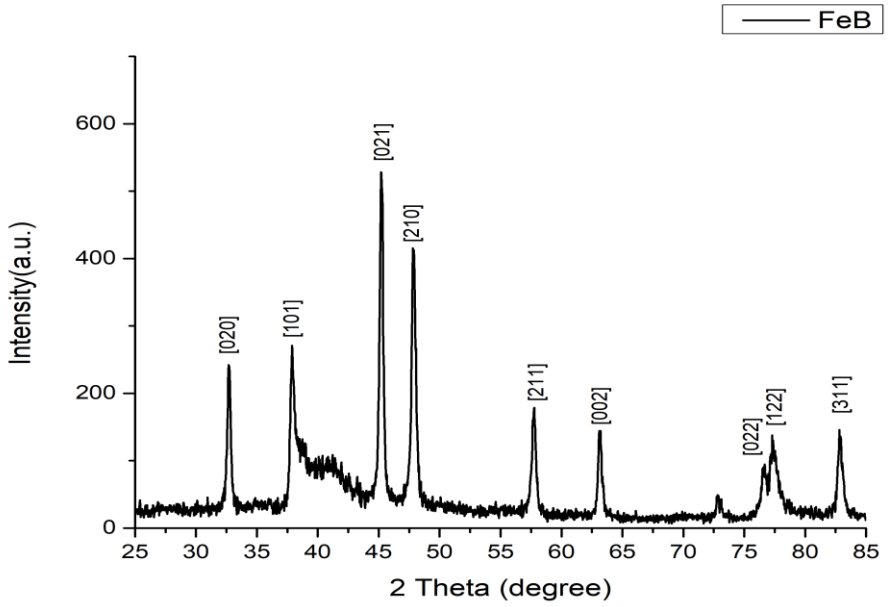

Figure 4.4. XRD pattern of FeB.

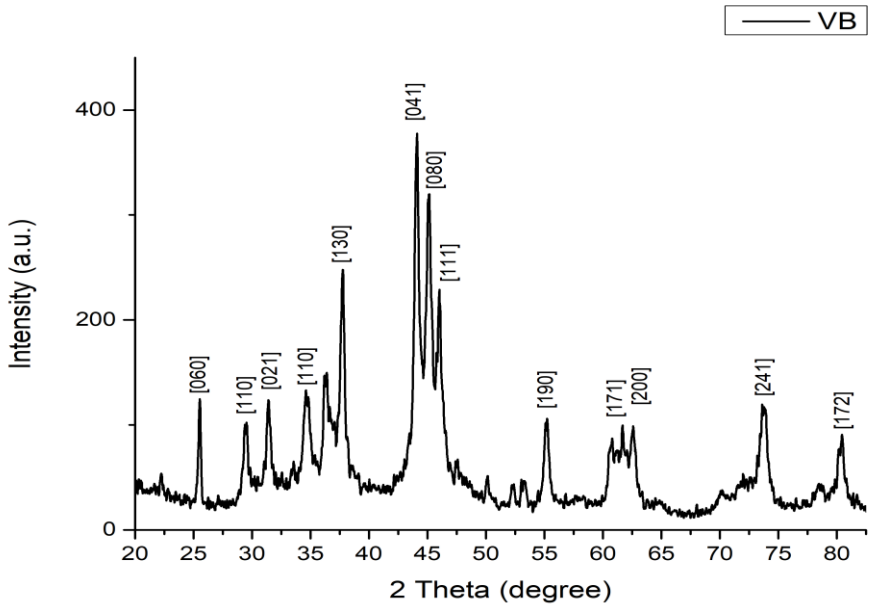

Figure 4.5. XRD pattern of VB.

Not only borides but also borates managed to be synthesized during this study to investigate their electrochemical properties. Yttrium borate (YBO_3) was synthesized by a solid-state method like borides. Fully crystalline powder was achieved as can be seen in fig. 4.6.

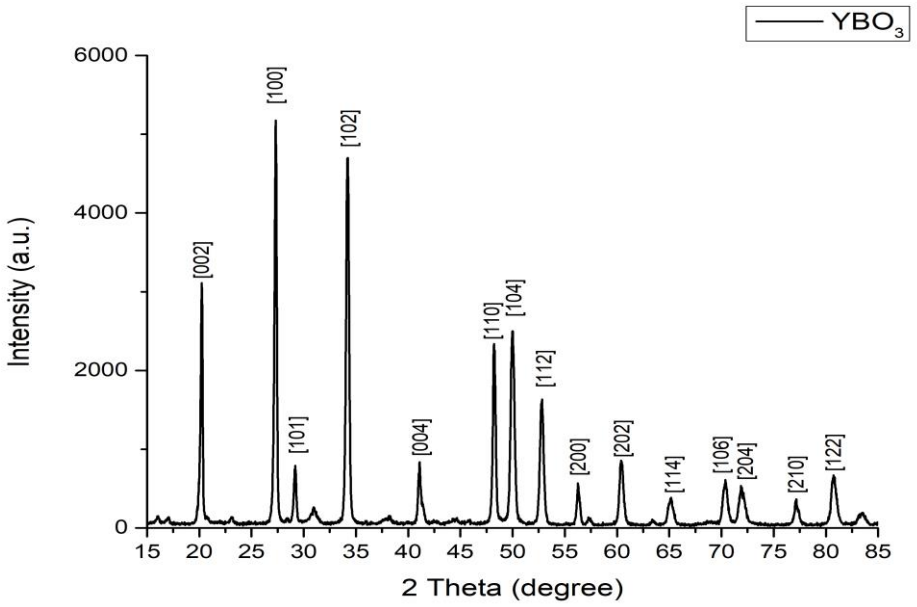

Figure 4.6. XRD pattern of YBO_3.

Synthesis of iron, vanadium, and molybdenum boride was also tried out during this study however it can not be achieved. Reactivity of boron source and transition metals that has multiple valency causes side reactions to occur during any process to synthesize any borides and borates. Manganese is the only metal that its boride and borate could be synthesized. Manganese borate was synthesized with the precipitation method as mentioned previously. In Figure 4.7 XRD pattern of $MnBO_3$ sample could be seen.

Rietveld analysis was also made on XRD patterns of all samples to show their fit between literature. Their symmetry and space group were pointed out with calculated lattice parameters given in Table 4.1.

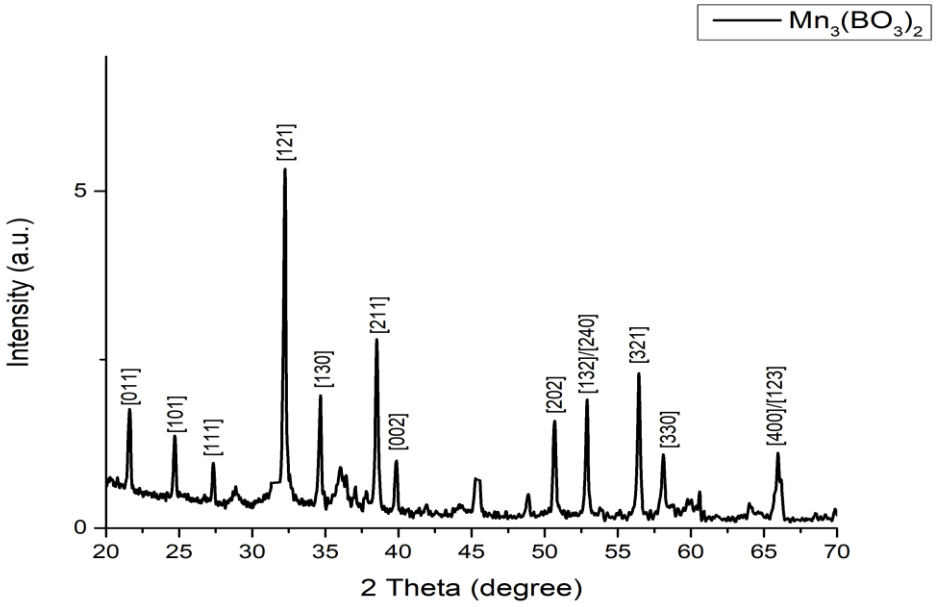

Figure 4.7. XRD pattern of $MnBO_3$.

Table 4.1 Rietveld analysis of synthesized borides and borates

Sample Name	*Material*	*Symmetry*	*Space Group*	*Lattice Parameter*			*%Rwp*
				a	*b*	*c*	
MoB	MoB_2	Hexagonal	P 6/m m m	3.053	-	3.092	15.97
FeB	FeB	Orthorhombic	P b n m	4.066	5.511	2.952	33.26
VB	VB	Orthorhombic	C m c m	3.057	8.061	2.978	25.5
MnB	MnB_2	Hexagonal	P 6/m m m	3.009	-	3.038	21.27
	MnB_4	Monoclinic	C 1 2/m 1	5.506	5.371	2.948	
$MnBO_3$	$Mn_2(BO_3)_2$	Orthorhombic	P n m n	5.681	8.713	4.655	22.86
YBO_3	YBO_3	Hexagonal	P 63/m	3.779	-	8.808	18.01

FeB had the least fit among all samples, it has 33.26 %Rwp. This is mainly caused due to degrees between 37.5 and 42.5. Three peaks of FeB structure can not be seen clearly at that range. The bump is observed covers peaks so that a good fit can not be achieved. It can be assumed that not fully crystallization of material was reason for that bump. Moreover, weight percentages of phases in the MnB sample were also

calculated with the Rietveld analysis. MnB_2 and MnB_4 have weight percentages of 56.94 % and 43.06 % in the sample, respectively.

The morphology of MnB was examined by SEM. It is seen that particles were coarse and agglomerated in Figure 4.7. The formation of agglomerates was expected since temperature synthesis is high enough. Two different phases in terms of morphology were not observed during the SEM examination.

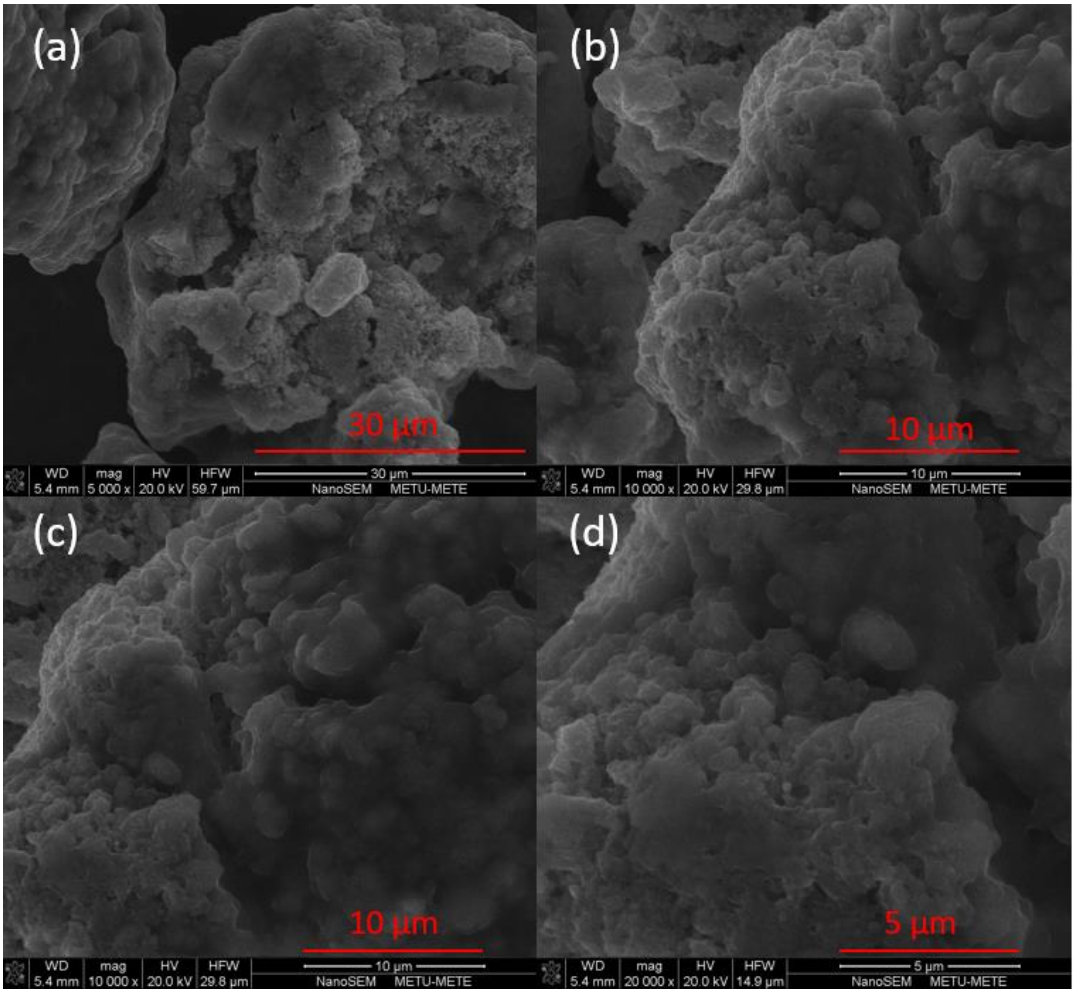

Figure 4.8. SEM images of MnB at (a) 5000x, (b, c) 10000x, and (d) 20000x magnifications.

FeB was also examined morphologically via SEM. In Figure 4.9. it is also agglomerated during synthesis, and smaller particles were observed inside agglomerates. Particles are observed to be more hollow than the manganese boride sample.

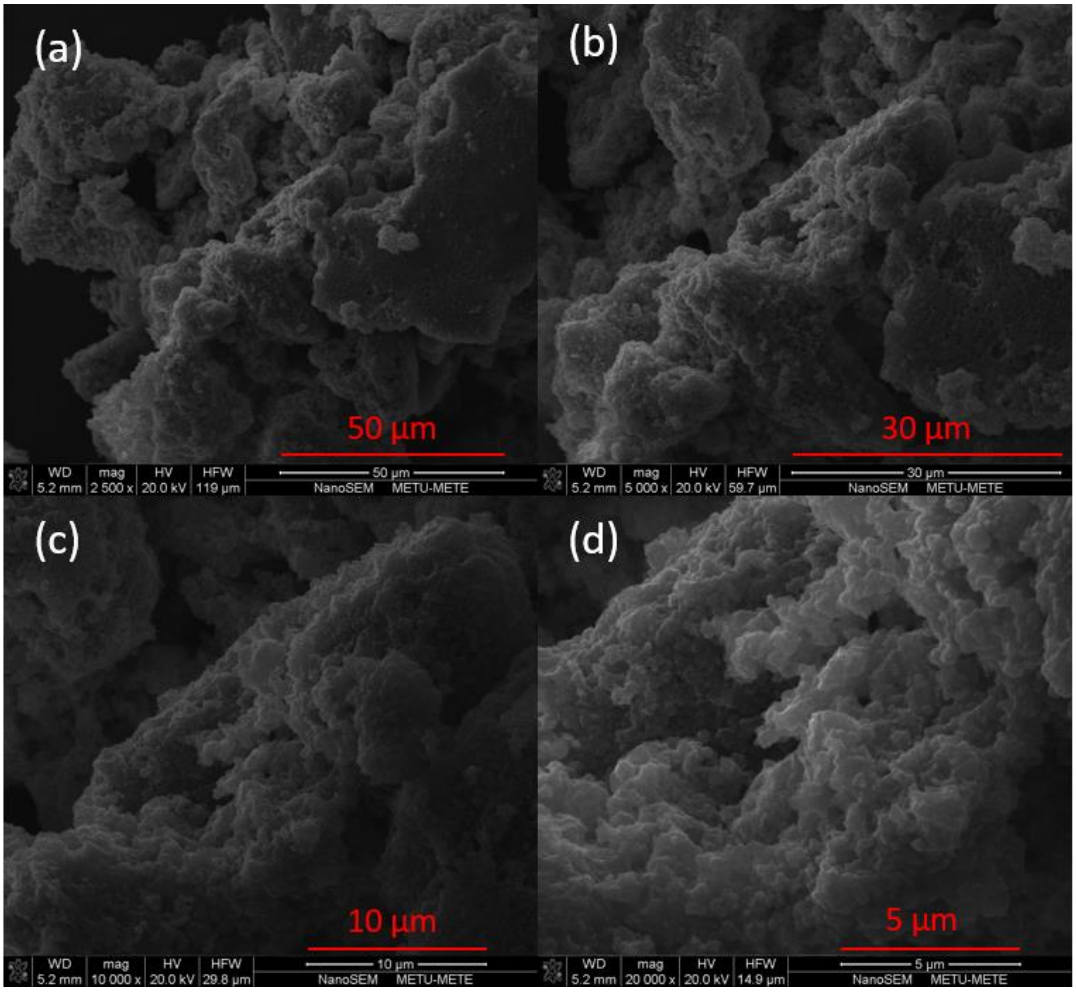

Figure 4.9. SEM images of FeB at (a) 2500x, (b) 5000x, (c) 10000x, and (d) 20000x magnifications.

Agglomerated particles of MoB are also witnessed in SEM images in Figure 4.10. It is seen that agglomerates are more hollowed than previously mentioned samples and large holes were observed on particles as well.

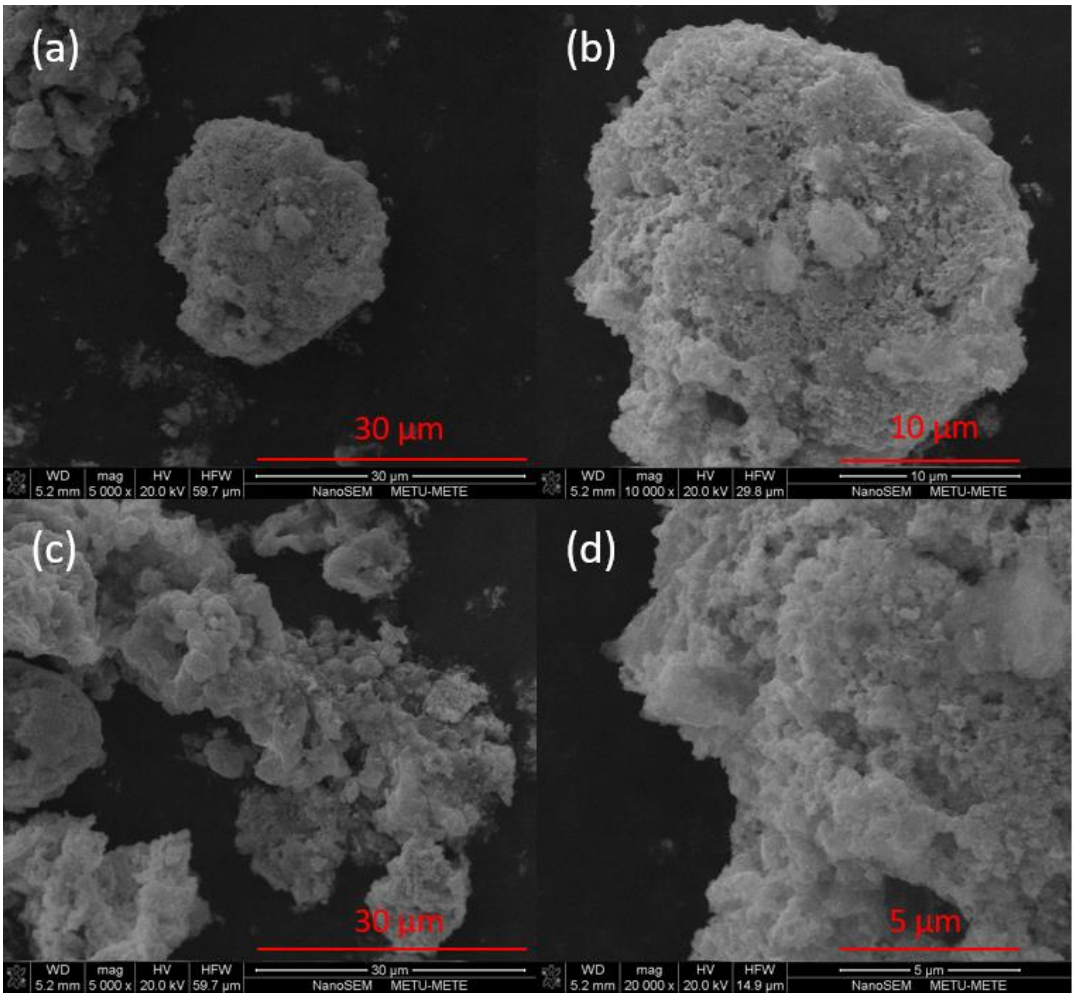

Figure 4.10. SEM images of MoB at (a, c) 5000x, (b) 10000x, and (d) 20000x magnifications.

A significant difference in the morphology of the VB sample was observed in Figure 4.11. Particles were not agglomerated as round shaped, and they are stacked as a layered structure. Holes are also observed on top and between layers.

Morphology of borates was examined via SEM as well. For both $MnBO_3$ (Figure 4.11) and YBO_3 (Figure 4.12), large agglomerates were also observed even if $MnBO_3$ was synthesized with the precipitation method. It is noted that borates are not as hollowed as boride samples. Moreover, it is noted that YBO_3 has a smooth surface than other samples with small cubic-like structures on particles.

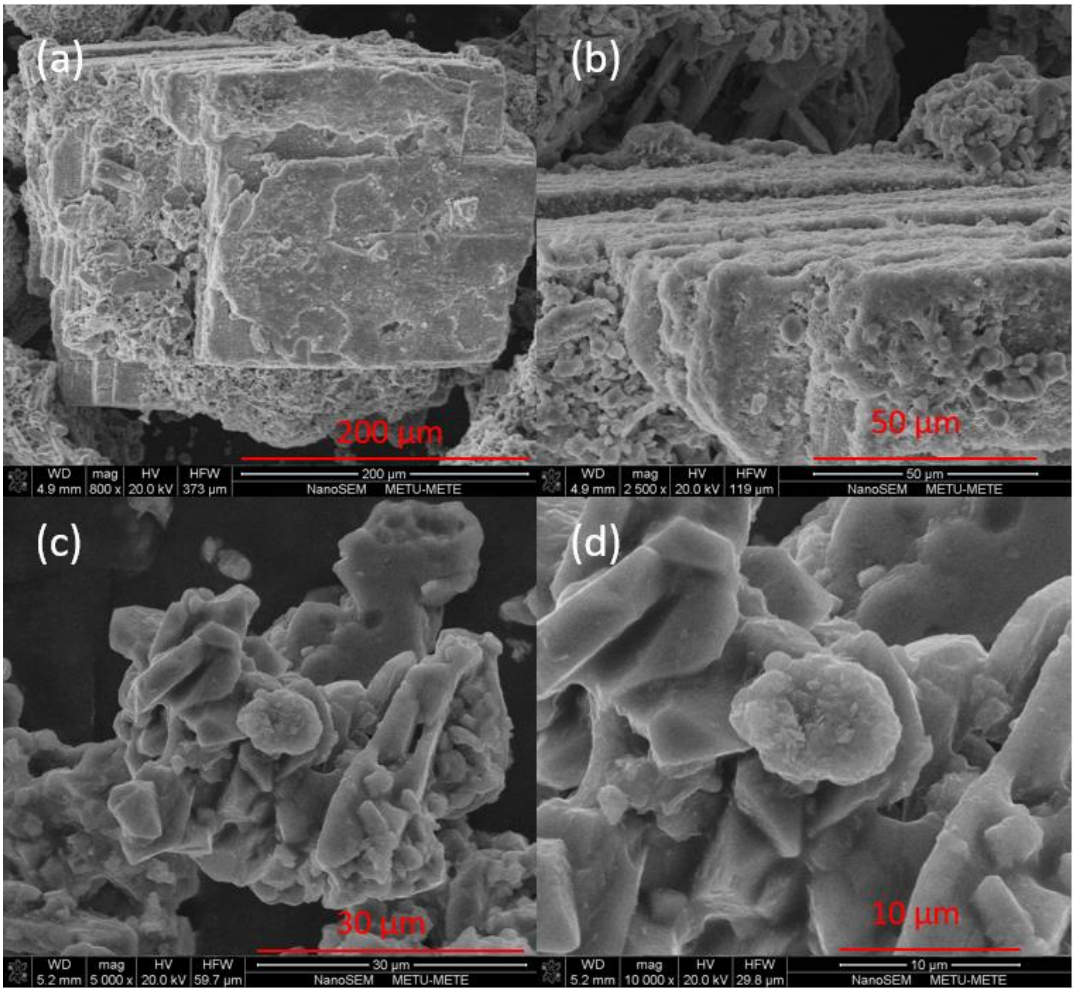

Figure 4.11. SEM images of VB at (a) 800x, (b) 2500x, (c) 5000x and (d) 10000x magnifications.

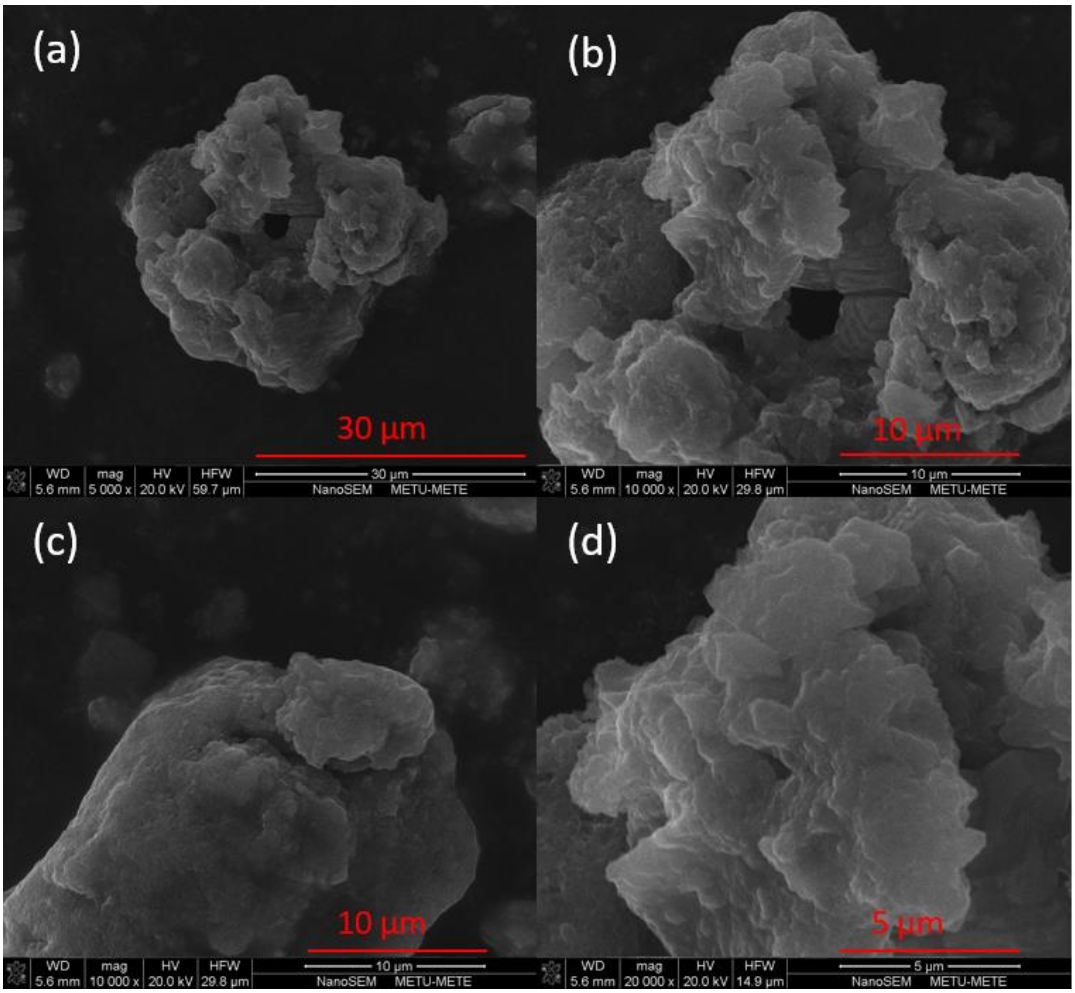

Figure 4.12. SEM images of $MnBO_3$ at (a) 5000x, (b, c) 10000x, and (d) 20000x magnifications.

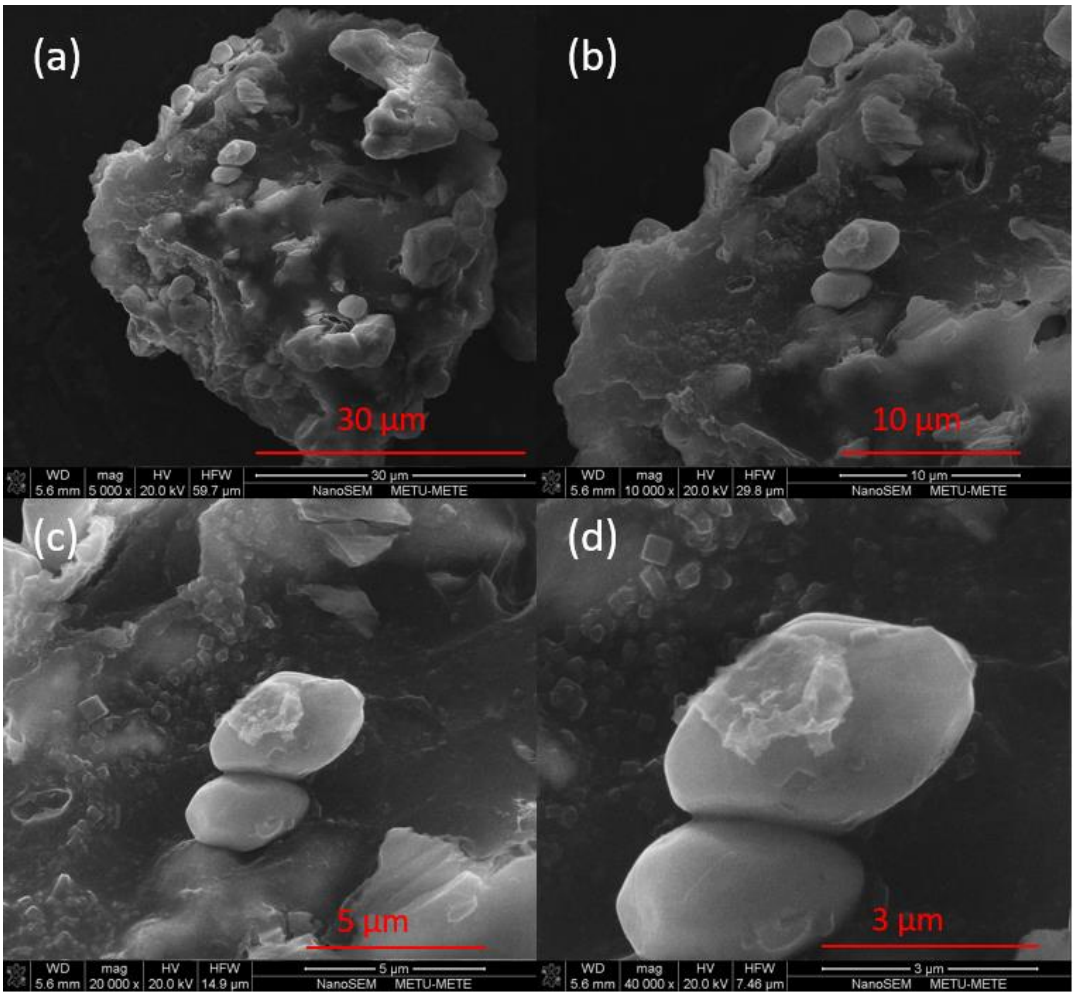

Figure 4.13. SEM images of YBO_3 at (a) 5000x, (b) 10000x, (c) 20000x and (d) 40000x magnifications.

4.2 Electrochemical Analysis Results

Synthesized anode active materials were electrochemically tested at button cell formation as described in the previous chapter.

4.2.1 Galvanostatic Charge-Discharge Tests

As synthesized materials were referred to as anode active, they were discharged at the initial cycle. Initial discharge capacities of synthesized iron, molybdenum, vanadium, manganese boride; yttrium, and manganese borate were shown in Figure 4.14 and Figure 4.15, respectively. It is clear that among all synthesized anode active boron-based materials, manganese boride showed the highest initial discharge capacity which is 576.80 mAh/g and yttrium borate has 78.54 mAh/g specific capacity as the lowest one. Specific capacities of borides at initial discharges are followed as 519.55, 408.18, and 322.14 for MoB, FeB, and VB, respectively. Molybdenum and manganese boride showed higher specific capacity at their initial discharge than corresponding borides. Their capacities are higher than commercial graphite. Although the capacity of iron boride is higher than graphite as well, the difference is not remarkable. Vanadium boride is the only material among synthesized borides that has a lower capacity initially than commercial anode material. On the other hand, its specific capacity is extremely higher than yttrium borate which has a specific capacity even lower than cathode active materials that are actively used. Its an expected result since yttrium borate is the heaviest material that was synthesized during this study. Manganese borate has a significantly higher initial discharge capacity than yttrium boride which is 493.98 mAh/g.

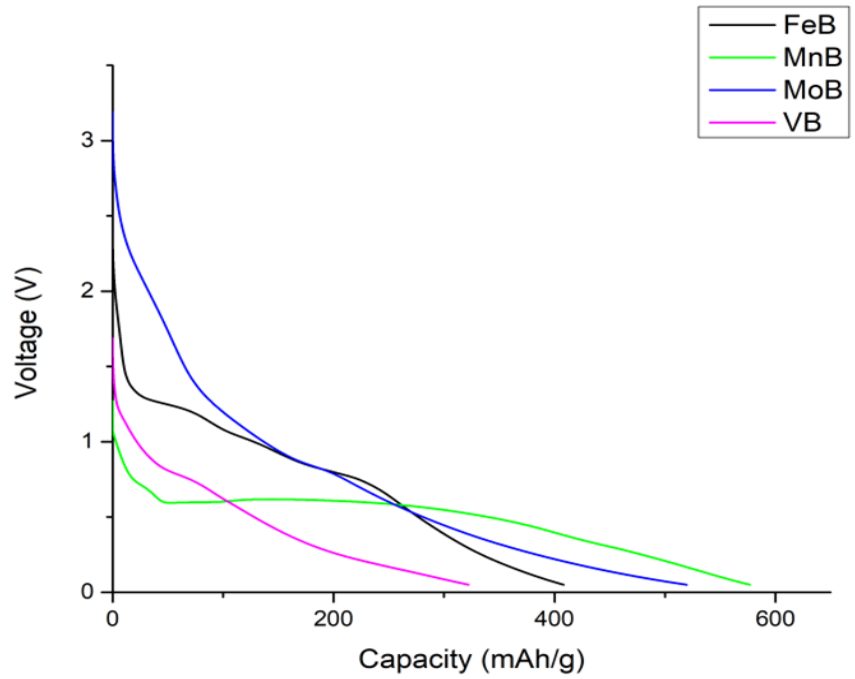

Figure 4.14. The initial discharge capacity of borides.

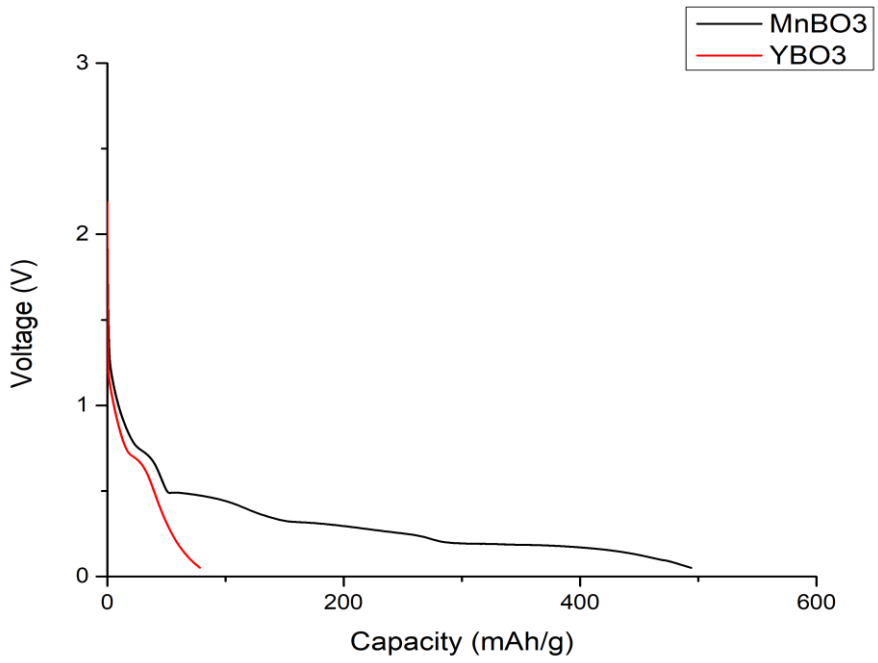

Figure 4.15. The initial discharge capacity of borates.

As mentioned before, the specific capacity of boron-based materials decays significantly after initial discharge. After initial discharges, borides and borates were cycled four times at 20 mA/g current density to observe that decay and report their actual capacities. A decrease in specific capacity was observed on all of the synthesized borides and borates. MnB noted as highest initial discharge capacity as 576.80 mAh/g. However, charge capacity was only 247.28 mAh/g which indicates that its colombic efficiency was only 42.9% in Figure 4.16. In the next cycles, capacity decrease continued but was not as severe as the first two cycles. For the second, third, and fourth cycles specific discharge capacity was measured as 251.34, 228.41, and 211.27 mAh/g while delivered charge capacities were 247.28, 218.56, and 207.34 mAh/g, respectively. The four charge and discharge cycles of MoB are shown in Figure 4.17. Similar to MnB capacity at first charge was less than initial discharge capacity. Charge capacity was obtained as 310.55 mAh/g and coloumbic efficiency was 59.8% which is remarkably higher than MnB. Following cycles delivered specific charge capacities of 310.55, 293.79, and 283.96 mAh/g while specific discharge capacities are obtained as 316.74, 296.43, and 283.02 mAh/g. respectively. Despite MoB having less specific capacity at initial discharge than MnB, it maintained its capacity over several cycles better than manganese boride. Colombic efficiency of FeB was calculated as 57.1% for the first charge/discharge in Figure 4.18. Specific charge capacities for several cycles were obtained as 233.07, 218.67, and 212.24 with specific discharge capacities as 238.10, 225.14, and 218.59, respectively. Despite measured capacities being much lower than the MoB sample, colombic efficiency and overall specific capacity of FeB were higher than MnB as well. The four charge and discharge capacities of VB were plotted in Figure 4.19. After initial charge and discharge, coloumbic efficiency was calculated as 68.5 which indicates that VB has the highest efficiency among all synthesized borides. Specific charge capacities are noted as 220.65, 185.65, and 183.49 mAh/g with discharge capacities of 209.47, 192.48, and 191.68 mAh/g respectively.

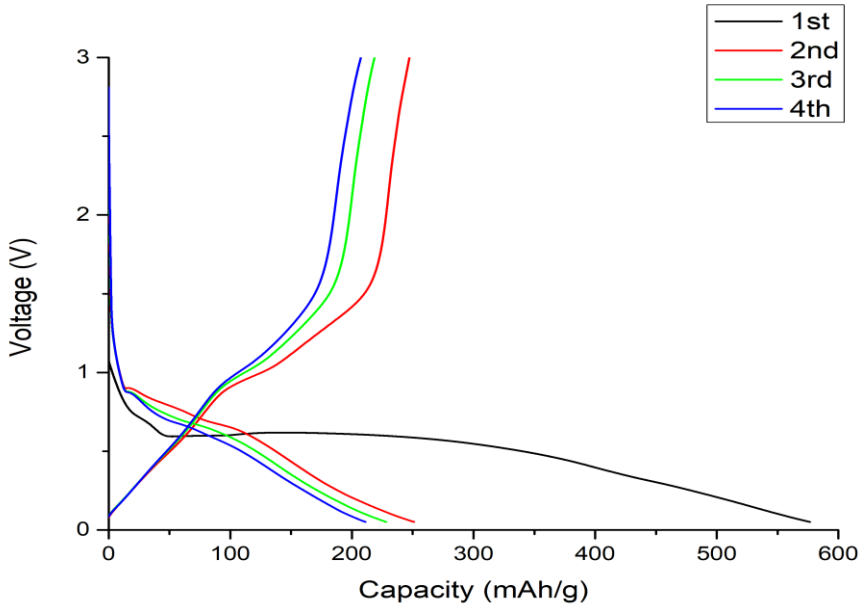

Figure 4.16. Charge/Discharge Cycles of MnB at 20 mA/g Current Density.

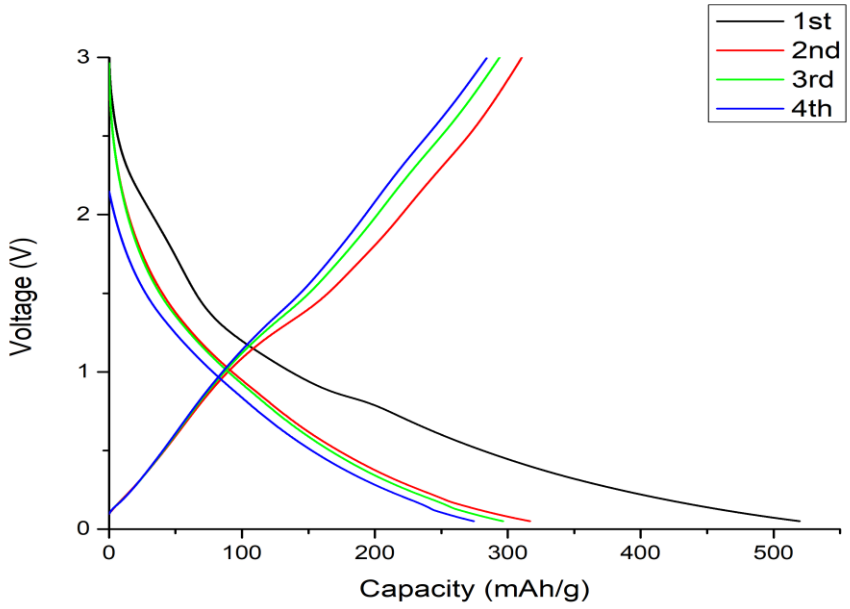

Figure 4.17. Charge/Discharge Cycles of MoB at 20 mA/g Current Density.

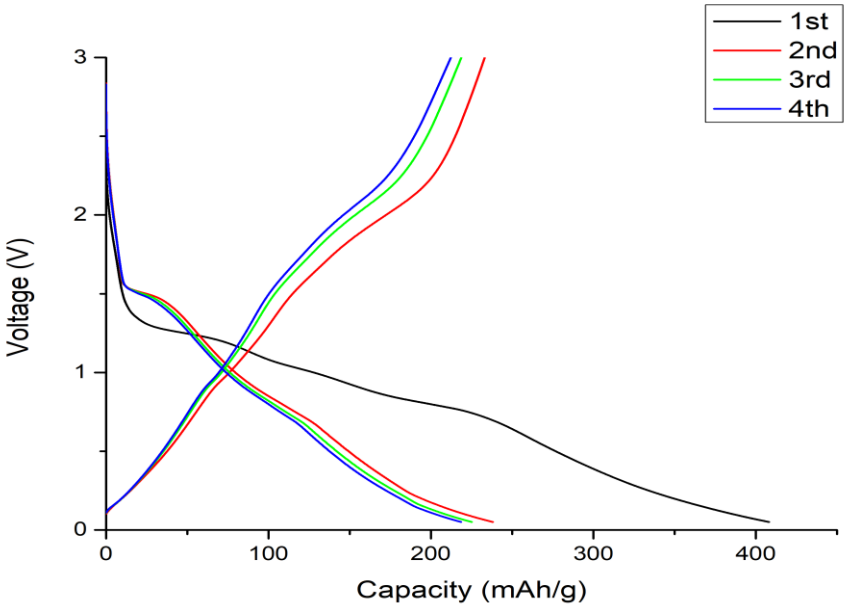

Figure 4.18. Charge/Discharge Cycles of FeB at 20 mA/g Current Density.

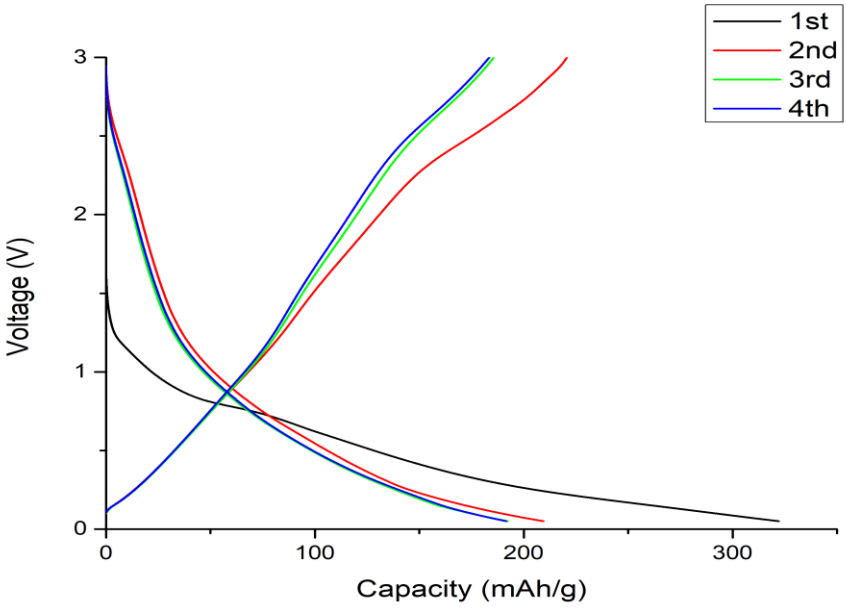

Figure 4.19. Charge/discharge cycles of VB at 20 mA/g current density.

Galvanostatic charge and discharge analysis to investigate capacity decrease and initial coloumbic efficiency also made on borates. $MnBO_3$ did not suffer as much as its counterpart boride in terms of coloumbic efficiency. It was calculated as 56.4% for initial charge and discharge in Figure 4.20. Specific charge capacities were measured for manganese borate as 278.43, 253.02, and 2.42.57 mAh/g where discharge capacities were 270.31, 254.37, and 244.79 mAh/g, respectively. Even if its initial discharge was noted as the lowest of all synthesized samples, YBO_3 also suffered from a capacity decrease after initial discharge as can be seen in Figure 4.21. Coloumbic efficiency for the initial cycle was calculated as 50.6%. Its specific capacities for all cycles are notably lowest of all, whereas it was less than any commercialized lithium-based cathode material. specific charge capacities were measured as 39.75, 37.67, and 36.76 mAh/g and discharge capacities were 41.35, 38.84, and 38.09 mAh/g, respectively.

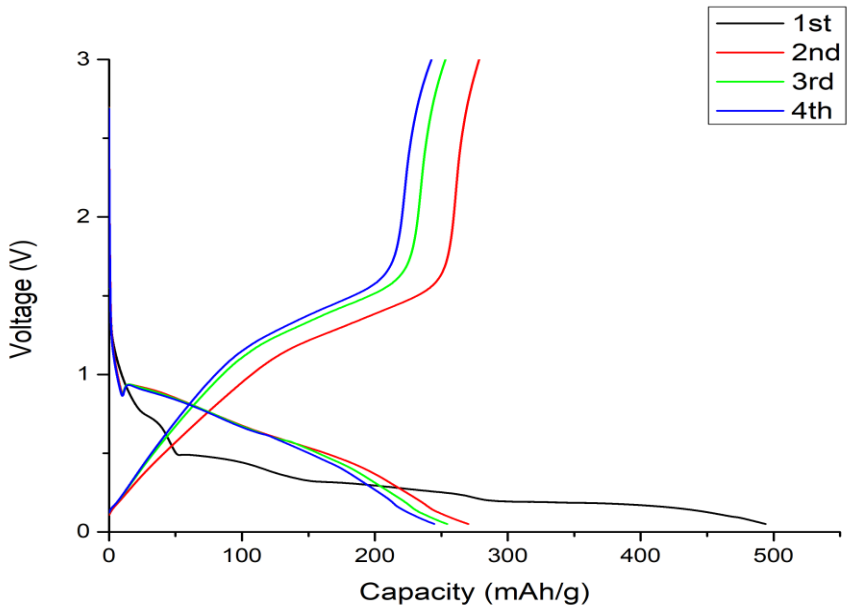

Figure 4.20. Charge/discharge cycles of $MnBO_3$ at 20 mA/g current density.

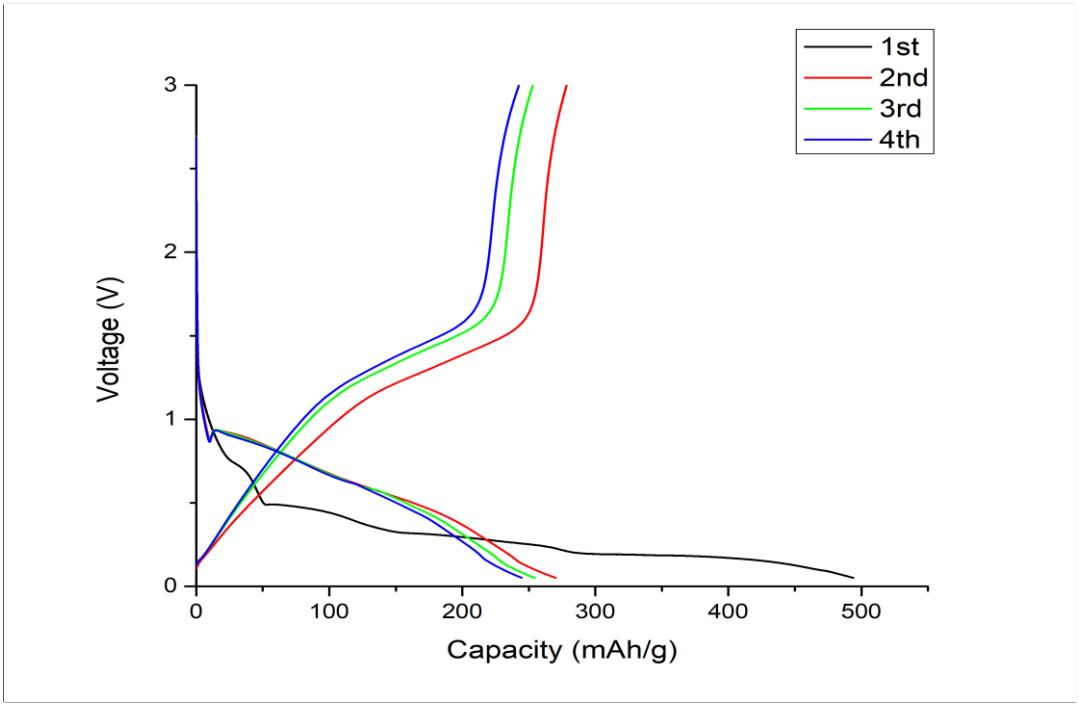

Figure 4.21. Charge/discharge cycles of YBO_3 at 20 mA/g current density.

Figure 4.22 shows the effect of charge/discharge rate on specific discharge capacities of borides. Borides samples were cycled five times at various current densities (20, 50, and 100 mA/g). Specific capacities of MnB, MoB, FeB, and VB were measured as 224.80, 293.27, 223.57, and 195.94 mAh/g, respectively (initial discharges were excluded) at 20 mA/g current density. With an increase at a current density to 100 mA/g capacity, a decrease was observed as expected. Since time given to lithium ions move in from bare lithium to anode material become less amount of stored decreases which outcomes a decrease in a specific capacity. MoB maintained the highest specific capacity of 210.12 mAh/g at the fastest current density which is remarkably more than other borides. After that, when the current rate decreased to the initial value of 20 mA/g, the MoB sample delivered 247.63 mAh/g discharge capacity. Although, the capacity of MoB after various rates decreased, it is still higher among all boron-based samples and also notably stable in the last three cycles.

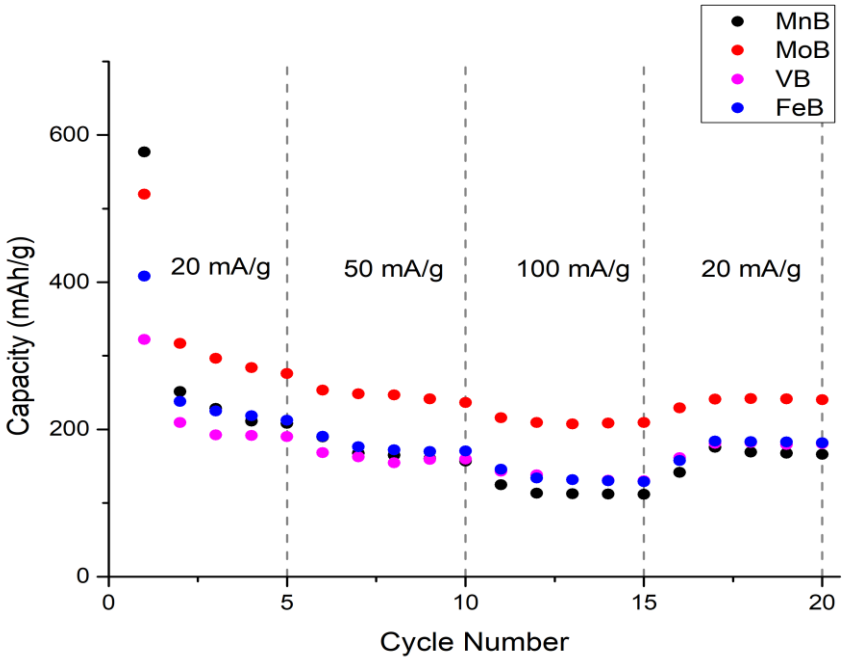

Figure 4.22. Rate capabilities of borides.

The rate capability of borates was also tested at previously mentioned current densities as can be seen in Figure 4.23. Specific capacities for $MnBO_3$ and YBO_3 were calculated excluding initial discharges as 251.93, and 39.15 mAh/g at 20 mA/g current density, respectively. The effect of the current rate on YBO_3 is not significant since obtained capacity even at a slow current rate is extremely low. The specific capacity of YBO_3 at 100m A/g is 27.98 mAh/g. On the other hand rate change affected $MnBO_3$ similar to borides. Around 100 mA/g decrease was observed between the slowest and fastest current rates. Despite the change in capacity being

noticeably high, $MnBO_3$ reached nearly the same capacity when it returned to 20 mA/g current density.

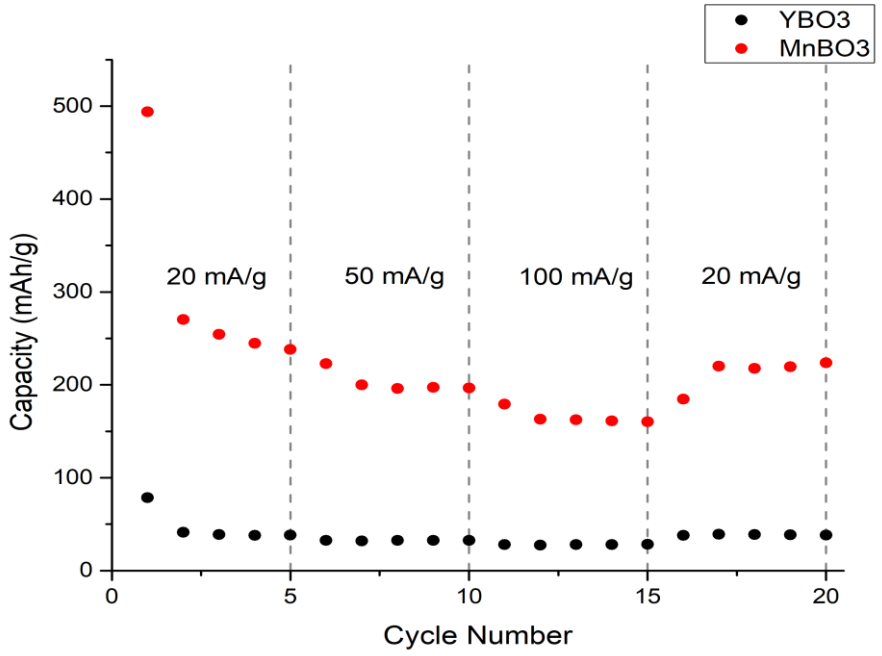

Figure 4.23. Rate capabilities of borates.

Cyclic stability of synthesized borides and borates was tested. Each sample was cycled fifty times at 20 mA/g current density to investigate the effect of cycle number on specific capacity. In the first ten cycles, capacities dropped drastically as can be seen in Figure 4.24. MnB suffered from a capacity drop more than other borides, after the last cycle, a specific capacity of 128.45 mAh/g was observed. Capacity conservation was calculated as 54.99% which indicates that MnB as the anode is not stable enough. Moreover, MoB also showed a capacity drop after cycles, 217.10 mAh/g specific capacity measured after fifty cycles. However, MoB showed the highest capacity among all samples with 73.55% capacity conservation. Although VB does demand high enough capacity to overcome the specific capacity of commercial anode materials, its capacity is close to lithium-based cathode with 85.37% conservation of specific capacity after 50 cycles. That makes VB most stable

between synthesized borides. The last cycle at specific capacity of 148.11 mAh/g was recorded for FeB. As a result, capacity retention of iron boride was calculated as 70.01% which makes it second lowest retention among boride samples.

Figure 4.24. Cyclic stability of borides at 20 mA/g current density after 50 cycles.

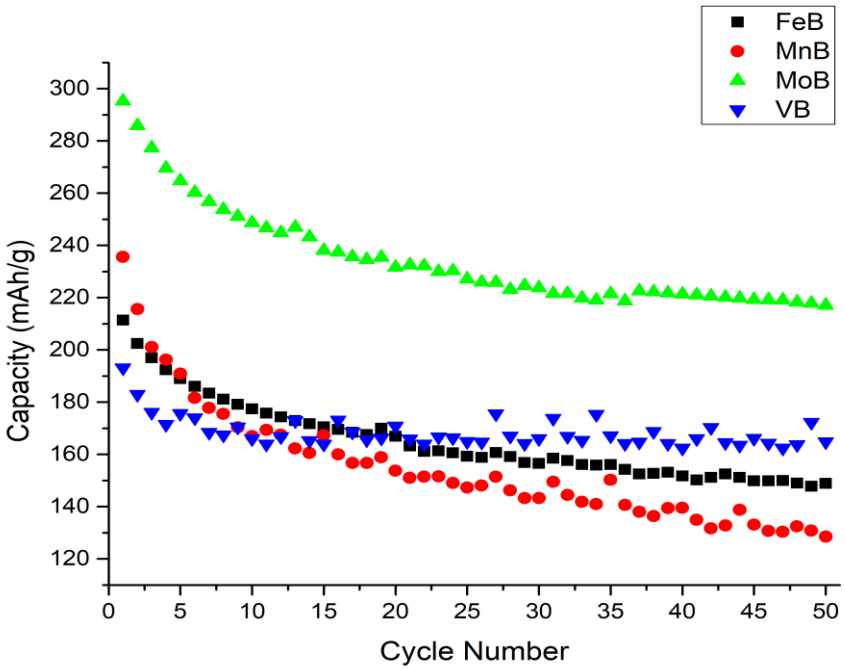

$MnBO_3$ showed similar behavior with manganese boride. As can be seen in Figure 4.25, a specific capacity of 342.49 mAh/g was recorded at the first cycle and capacity dropped to 141.20 mAh/g after fifty cycles which means that capacity conservation was only 41.23%. YBO_3 had the highest capacity conservation which is 84.48% among all samples that are synthesized during this study. Even though conservation was notably high, its specific capacity drastically low.

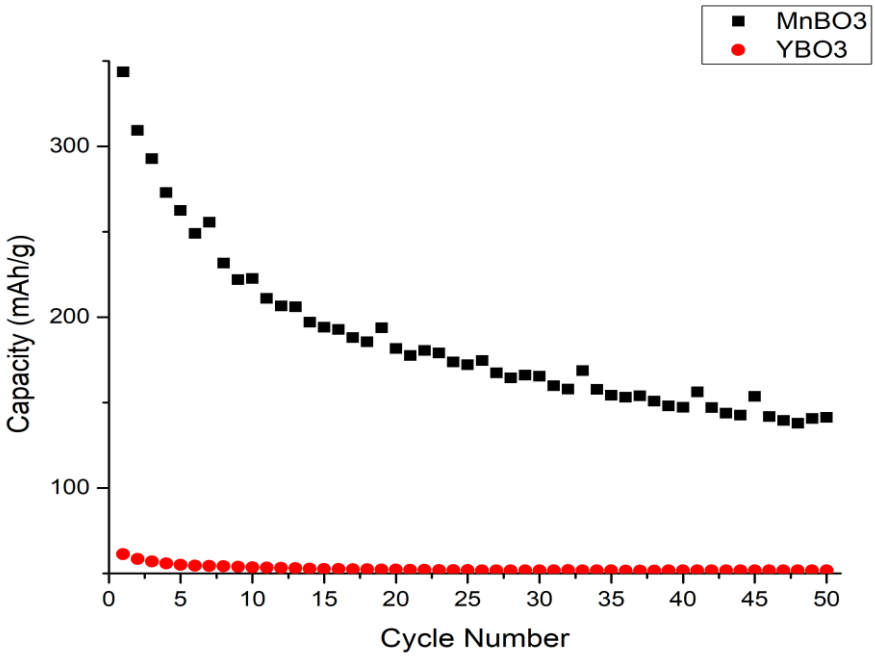

Figure 4.25. Cyclic stability of borates at 20 mA/g current density after 50 cycles.

4.2.2 Cyclic Voltammetry

Cyclic voltammetry was performed to understand the charge-discharge process as well as the reasoning for capacity decrease throughout it. A sharp peak at 0.78 V followed by a bump to 0.02 V was observed during the initial discharge cycle of every sample at 0.02 mV/s speed. Decomposition of electrolyte combined with the formation of SEI layer occurs during that irreversible reaction[34]. SEI formation causes loss of active materials as a result capacity drop occurs. That explains the reasoning for capacity decrease which was observed at galvanostatic charge and discharge.

4.2.2.1 MoB

Three cycles of cyclic voltammetry of MoB can be seen in Figure 4.26. There is an irreversible peak observed at the initial CV cycle at 0.79 V which indicates decomposition of electrolyte with solid electrolyte interface formation. With supporting data of galvanostatic cycles which did not have any sharp slope change with constant voltage profile at charge and discharges of MoB, it could be claimed that intercalation occurs during lithiation and delithiation of molybdenum diboride. With the increase in scan rate, redox peaks that imply lithiation and delithiation of lithium became more obvious in Figure 4.27. Redox reactions during lithiation and delithiation of MoB occur at 1.25 and 1.45 V, respectively[31].

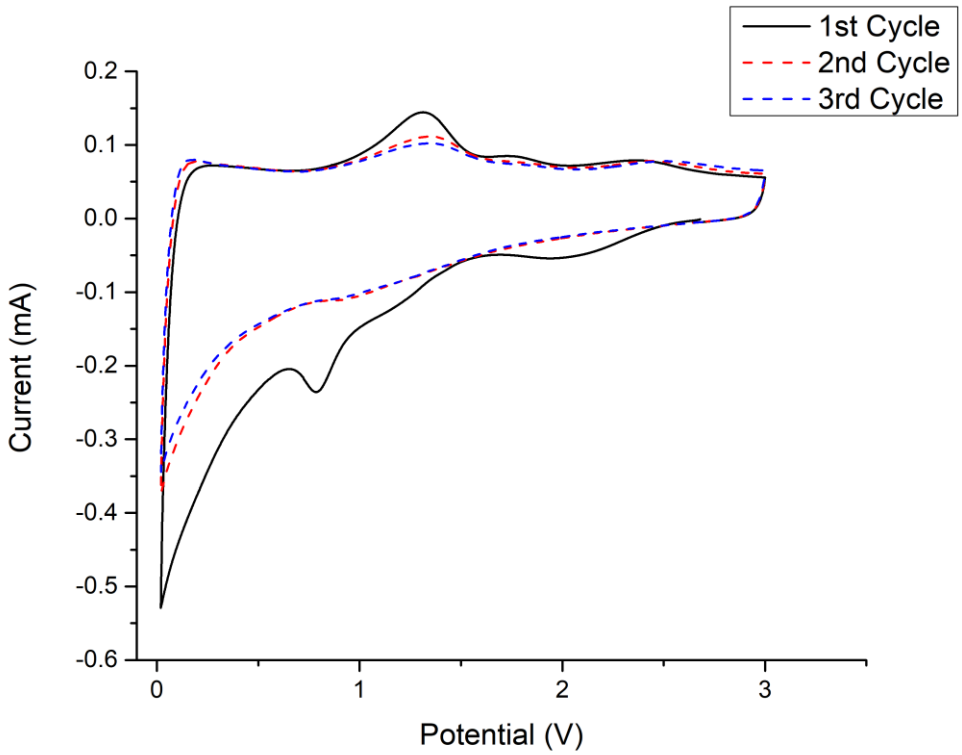

Figure 4.26. Cyclic voltammetry of MoB at 0.0 2mV/s scan rate.

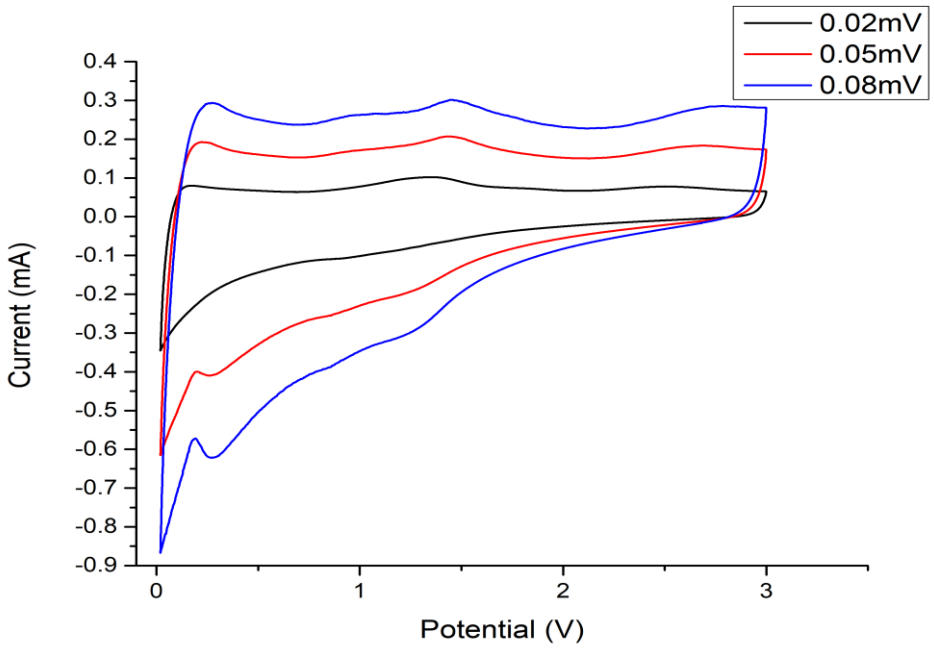

Figure 4.27. Cyclic voltammetry of MoB at 0.02, 0.05, and 0.08 mV/s scan rate.

4.2.2.2 FeB

Iron boride showed characteristic peaks upon CV at 0.02 mV/s scan rate in Figure 4.29. Solid electrolyte interface formation was observed as a reduction peak at 0.75 V like the MoB sample. With the increase in scan rate, two nearly overlapped peaks were separated slightly in Figure 4.28. It was obvious that three distinguished peaks were observed during reduction at 1.45, 0.81, and 0.70 V. These reductions were followed by three oxidation peaks at 0.96, 1.61, and 2.04 V. As can be seen at various cycles after the initial one, these redox peaks overlap on each other which indicates reversibility. In general iron based anodes at Li-ion batteries show multistep lithiation and delithiation mechanism[38,39]. As a result, it was assumed that redox

peaks that were observed throughout cyclic voltammetry of FeB are related to multistep lithium insertion and deinsertion.

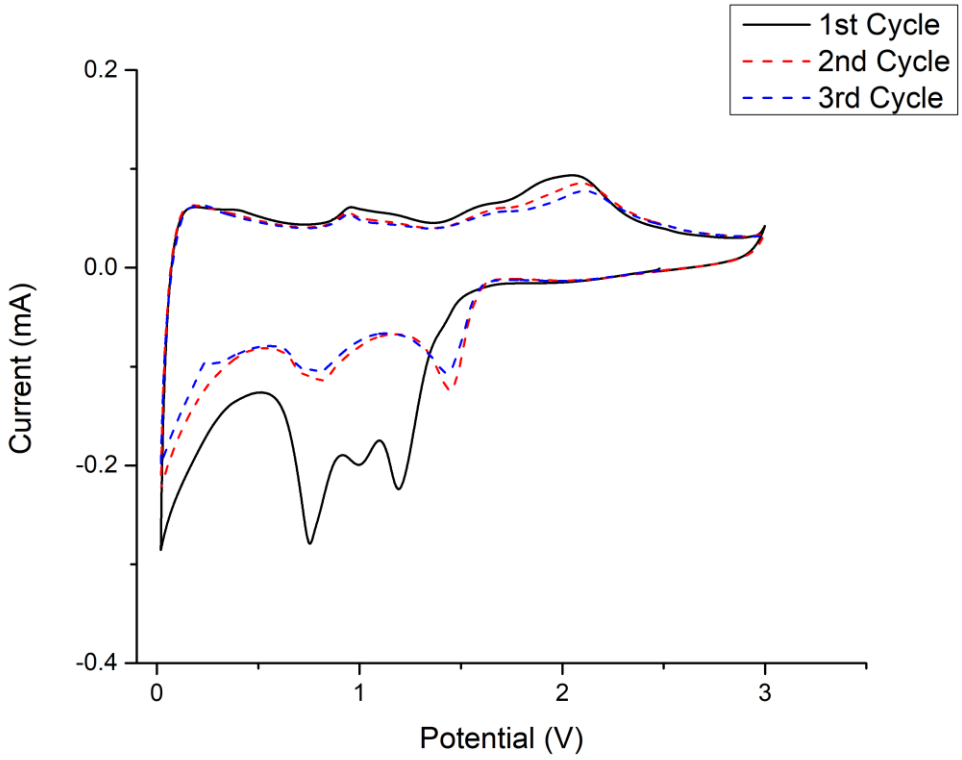

Figure 4.28. Cyclic voltammetry of FeB at 0.02 mV/s scan rate.

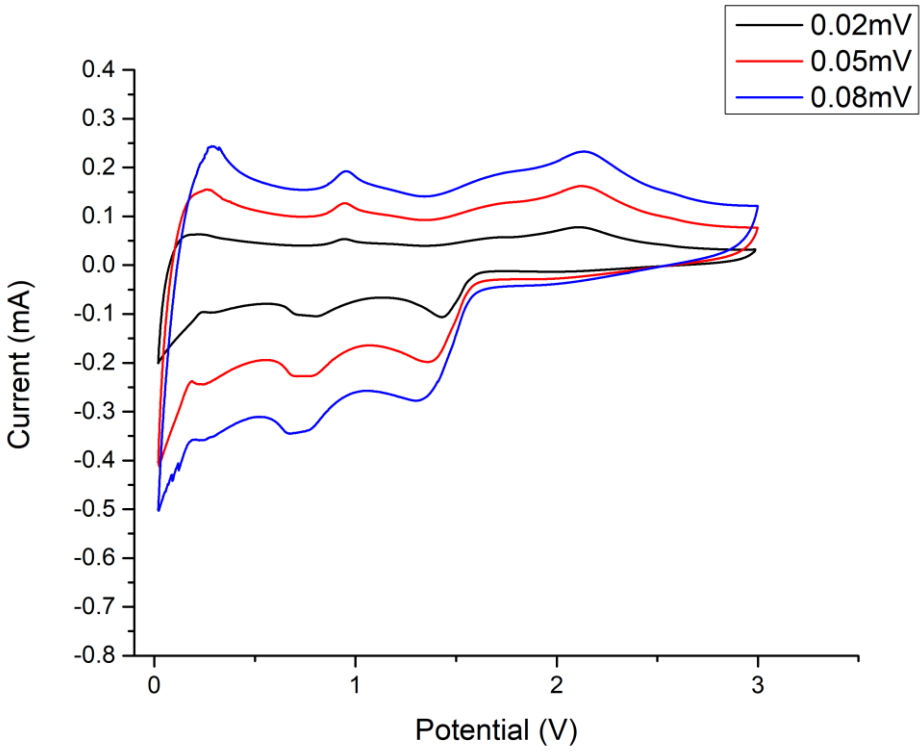

Figure 4.29. Cyclic voltammetry of FeB at 0.02, 0.05, and 0.08 mV/s scan rate.

4.2.2.3 VB

Formation of SEI was also observed at 0.74 V during reduction at the initial cycle in Figure 4.30. In addition to that, there was a reduction peak at 1.24 V, as the cyclic process continues that reaction was diminished. Within the increase, at scan rate, redox reactions become more noticeable in Figure 4.31. Reduction reactions at 2.35, 0.83 V as well as oxidation peaks at 0.91, 1.76, and 2.71 V were observed. As the peaks continued to overlap throughout cycles it is assumed that these were related to intercalation and deintercalation. It is known that lithiation of vanadium-containing anodes occurs with a multistep process. That explains the multiple redox couples observed at CV[40,41].

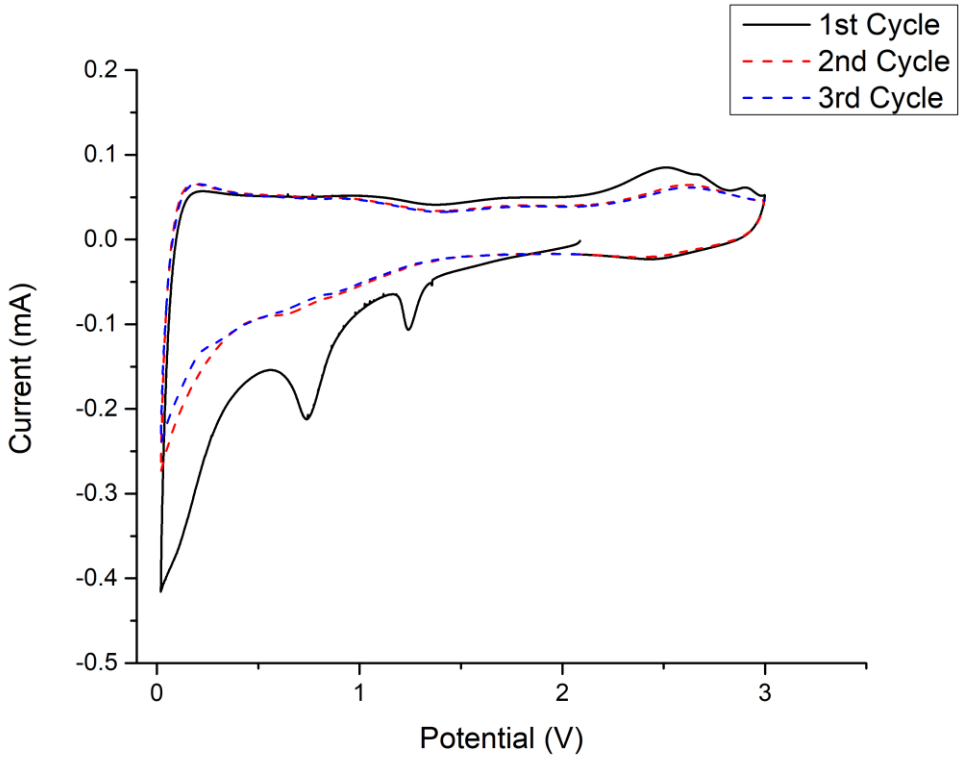

Figure 4.30. Cyclic voltammetry of VB at 0.02 mV/s scan rate.

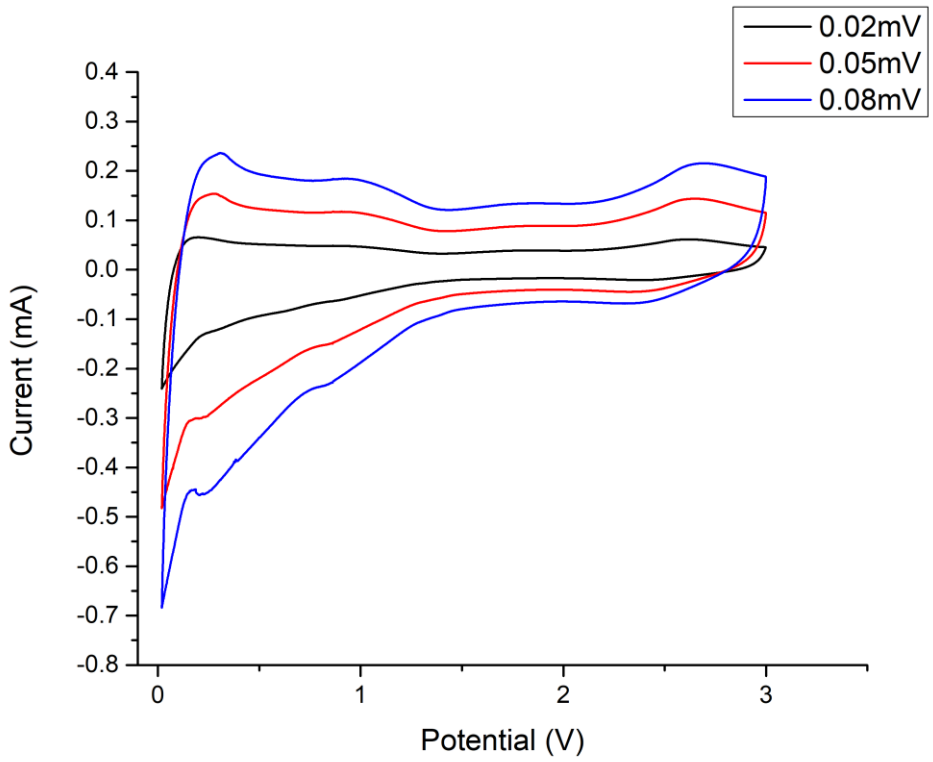

Figure 4.31. Cyclic voltammetry of VB at 0.02, 0.05, and 0.08 mV/s scan rate.

4.2.2.4 MnB

CV of MnB sample showed a difference from other borides. In addition to the SEI formation reaction at 0.74 V, there was a characteristic irreversible peak around 0.47 V observed. It is known that the reduction of manganese-containing materials to metallic Mn occurs during the delithiation of cells[42,43]. It was assumed that the peak at 0.47 V corresponds to the formation of metallic Mn with lithium boride. As cycles continued that irreversible peak completely disappears in Figure 4.32. The current change was not observed during the delithiation of the sample from 1.5 V to 3.0 V as well as lithiation from 3.0 V to 1 V. There were two distinct redox couples observed after the first cycle. Reduction peaks at 0.84 and 0.57 V, oxidation peaks at 1.03 and 1.39 V continued to overlap in the following cycles in Figure 4.33. Two

different redox couples were observed throughout cycles since there were two different manganese borides within the MnB sample.

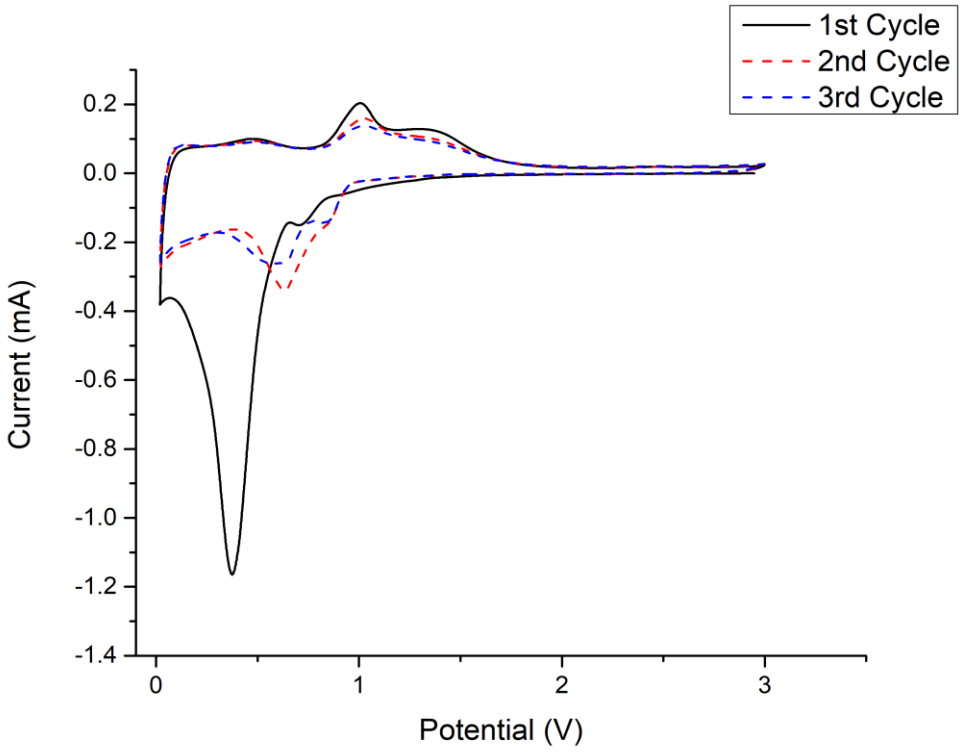

Figure 4.32. Cyclic voltammetry of MnB at 0.02 mV/s scan rate.

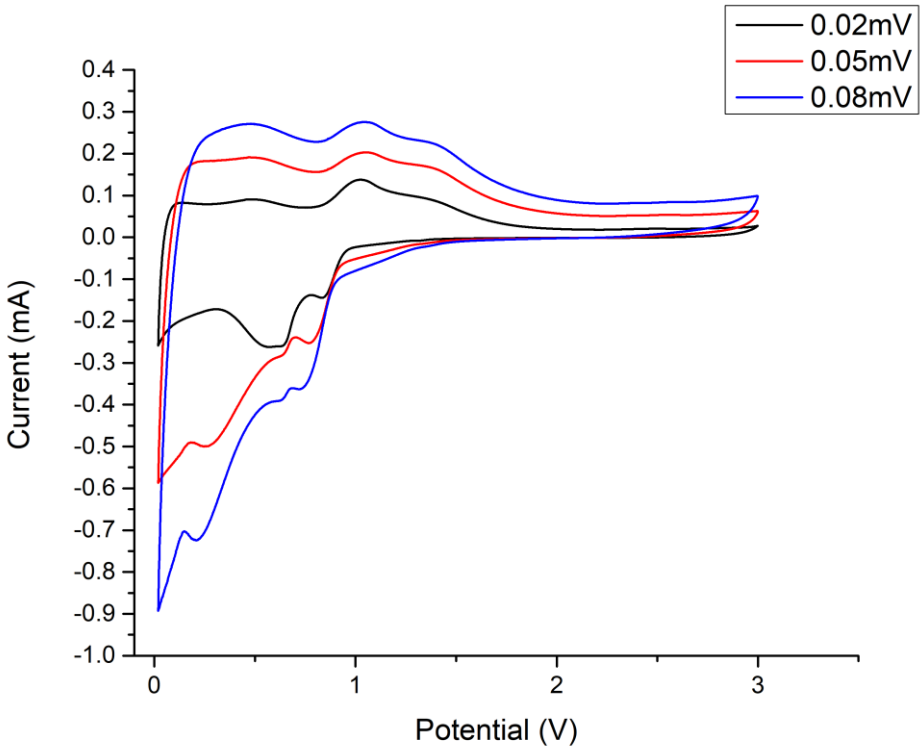

Figure 4.33. Cyclic voltammetry of MnB at 0.02, 0.05, and 0.08 mV/s scan rate.

4.2.2.5 $MnBO_3$

SEI formation at $MnBO_3$ was observed at 0.75 V which is similar to other samples. A sharp peak below 0.10 V was noted as a reduction of Mn^{2+} to manganese metal in Figure 4.34. A corresponding reaction the oxidation of metallic manganese to manganese oxide during delithiation of the cell was observed at 1.49 V. Moreover, the peaks of the following cycles correspond to the transformation of manganese shifted and the sharpness of peaks decreased as well. After the first cycle peaks, they continued to be overlapped throughout cycles and different scan rates in Figure 4.35. Redox reactions of cell occur at 0.70, 0.40 V and 1.38, 1.51 V, respectively. As a result of that reaction, B_2O_3 formed irreversibly which caused a loss of active material. That explained the loss of capacity throughout charge and discharge of $MnBO_3$ anode[42].

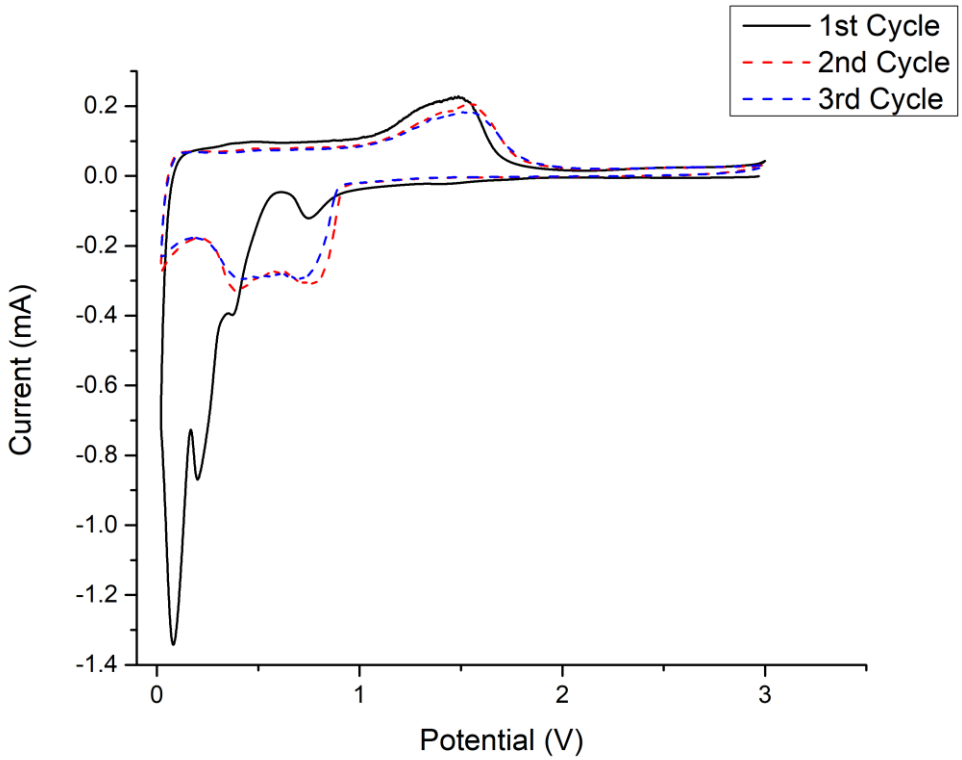

Figure 4.34. Cyclic voltammetry of $MnBO_3$ at 0.02 mV/s scan rate.

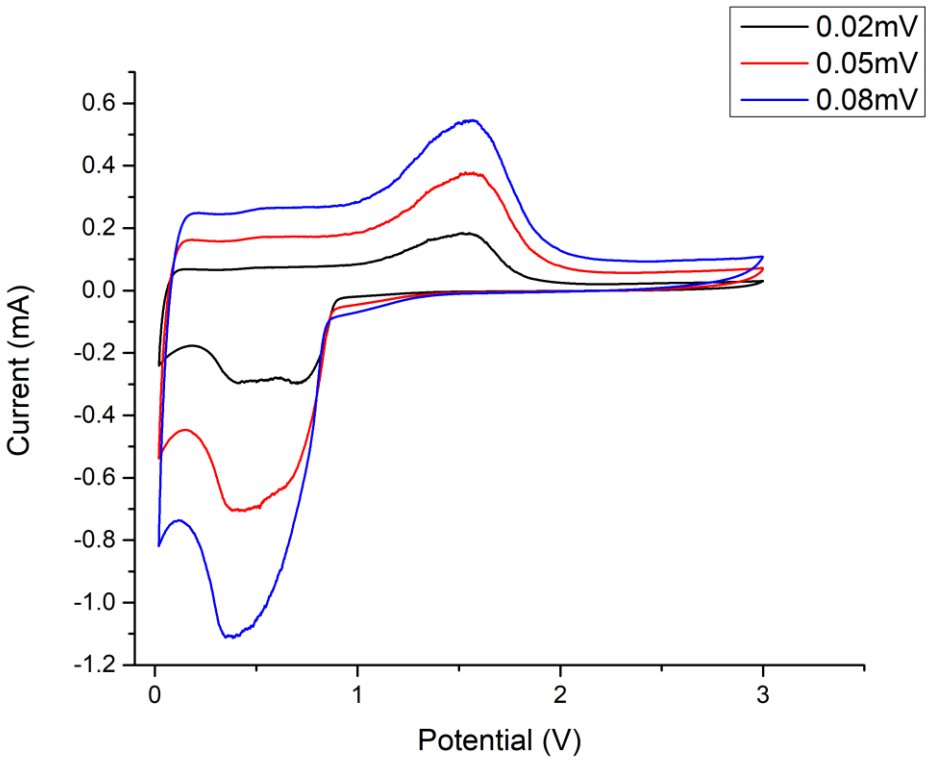

Figure 4.35. Cyclic voltammetry of $MnBO_3$ at 0.02, 0.05, and 0.08 mV/s scan rate.

4.2.2.6 YBO_3

In terms of electrochemical reaction voltage range, YBO_3 showed similar behavior as $MnBO_3$ and MnB. Similar to other yttrium-containing anodes, there was not any redox reaction observed over 1.50 V in Figure 4.36[44]. At 0.74 V, SEI formation was also observed like previous samples. Overlapped reduction peak at 0.91 V and oxidation peak at 0. 95 V was observed at various scan rates in Figure 4.37. This redox reaction was assumed to be related to lithiation and delithiation of lithium throughout the charge/discharge of YBO_3.

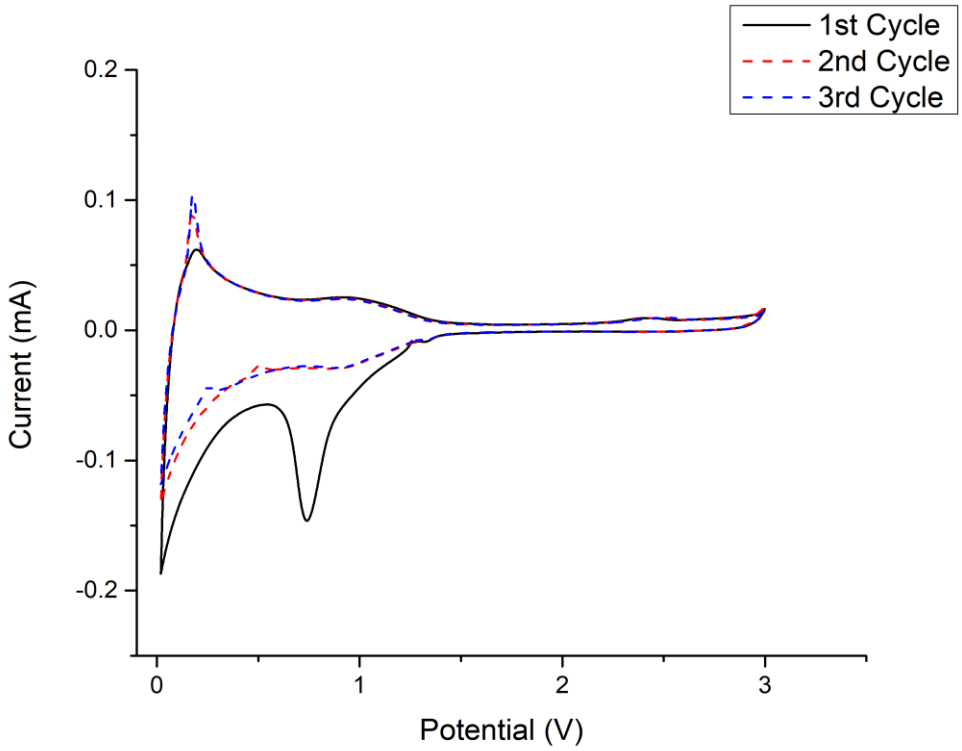

Figure 4.36. Cyclic voltammetry of YBO_3 at 0.02 mV/s scan rate.

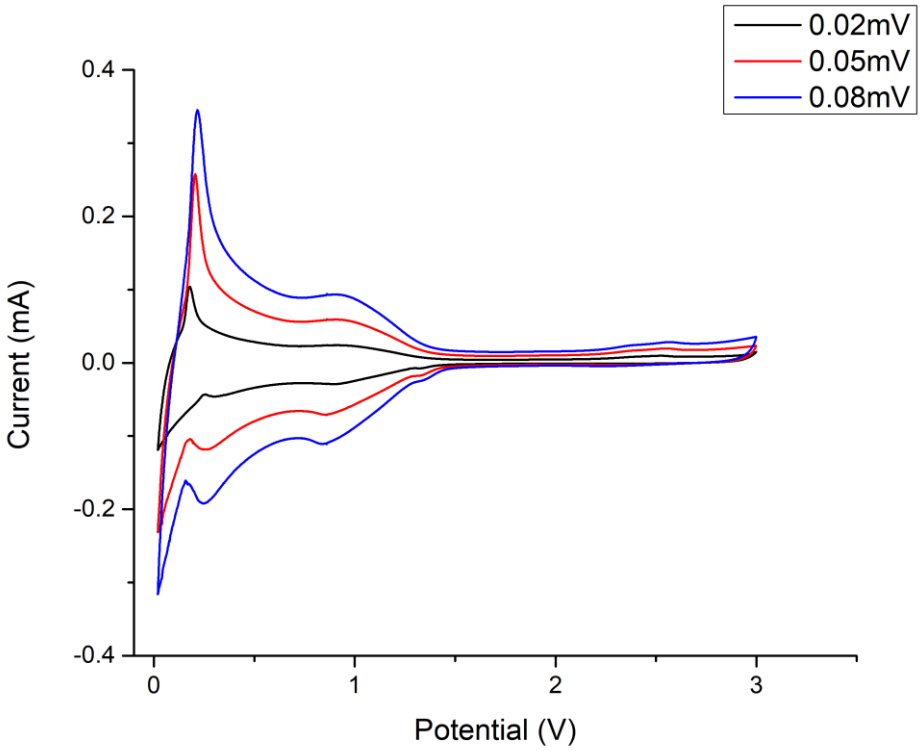

Figure 4.37. Cyclic voltammetry of YBO_3 at 0.02, 0.05, and 0.08 mV/s scan rate.

4.2.3 Physical Characterization of Cells

To understand what happens after lithiation of samples that have the highest and lowest capacity, cells that cycled several times were taken out of button cell configuration at the fully discharged condition and removed from copper foil to make XRD analysis. YBO_3 maintained its crystallinity fully in Figure 4.38.

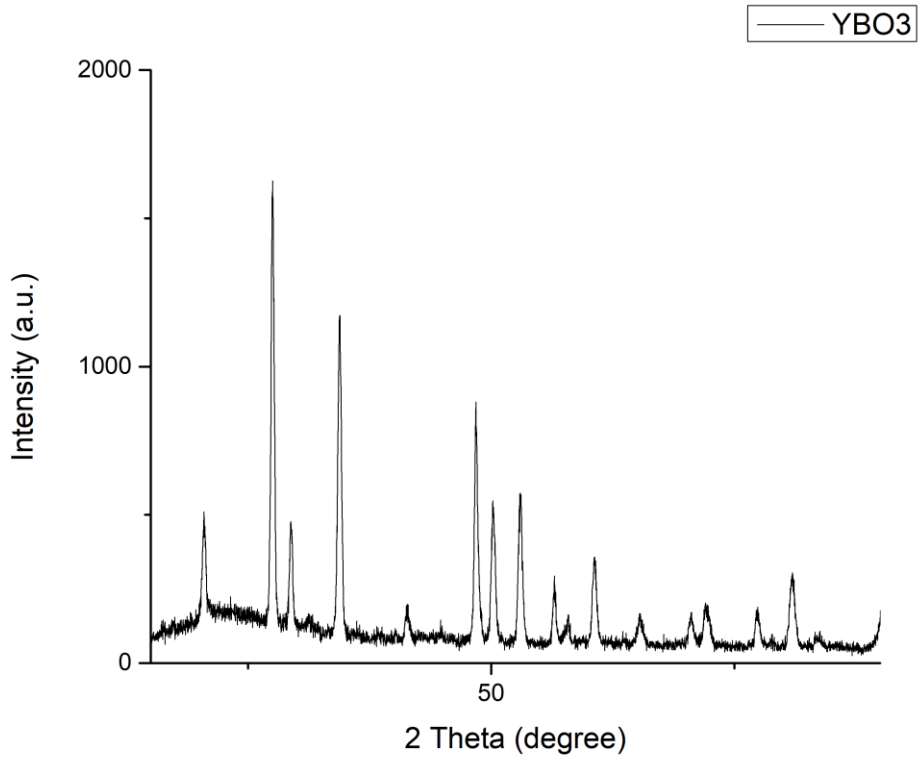

Figure 4.38. XRD pattern of fully discharged YBO_3.

MoB sample suffered from structural deformation after lithiation. Although there was a bump that indicates amorphization, it can also be seen that the crystallinity of the material was protected to a certain extent after the discharge process in Figure 4.39. There was no formation of any lithium boron-based material observed in the lithiated sample. That outcome also supports the results of CV in which there was not any chemical transformation during charge-discharge of MoB.

XRD analysis was also made on other samples. Decrease of crystallinity was observed for almost all samples however, results were not presentable enough for this study.

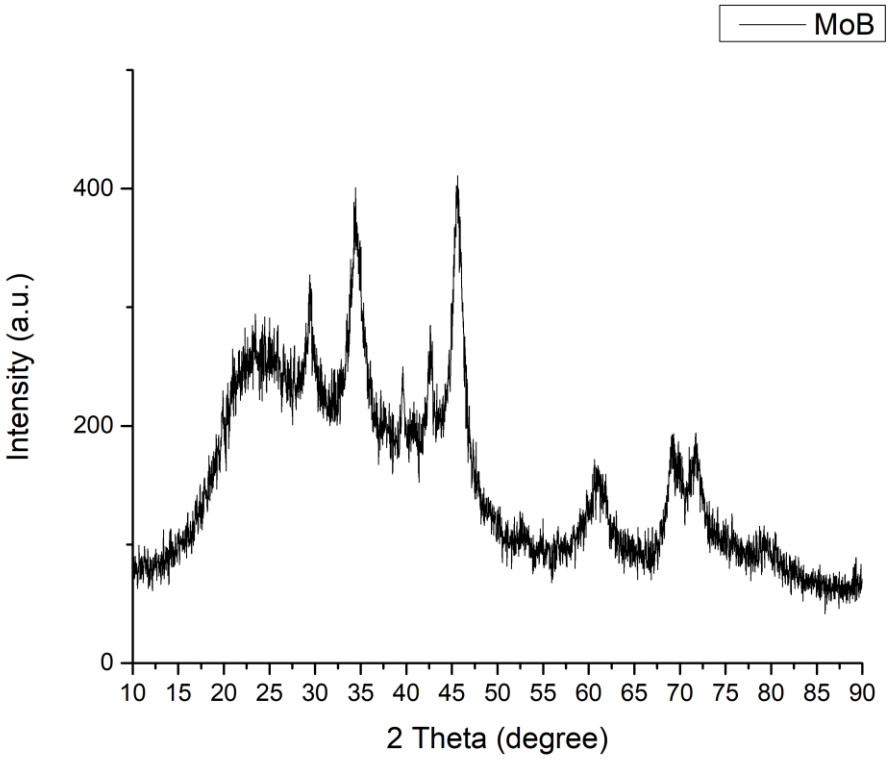

Figure 4.39. XRD pattern of fully discharged MoB.

CHAPTER 5

CONCLUSION

Extension of electrochemical knowledge on borides and borates, this study aimed to synthesize metal borides and borates to examine their properties as anode material in a lithium-ion battery.

The synthesis of iron, vanadium, molybdenum, manganese boride, and yttrium borate was managed by the solid-state synthesis method. During preliminary tests, 500, 700, and 900 ºC were tested as synthesis temperatures for borides. The synthesis temperature was chosen as 900 ºC since at 500 ºC metal oxide was not reacted with $NaBH_4$ and at 700 ºC even though the formation of sodium metaborate was observed there was not any metal boride formation.

Successfully synthesized four borides and two borates were tested with galvanostatic charge and discharge to measure their capacities and the effect of the rate change on capacity and stability. Initial discharge capacities of materials except YBO_3 were remarkably high enough to compete with commercial graphite, large capacity drops were observed for all samples. MnB with 576.80 mAh/g specific discharge capacity at initial discharge was the highest capacity among materials that are synthesized. On the other hand, a specific capacity of 78.54 mAh/g was recorded as the lowest among all samples. After initial discharges, extreme capacity drops were observed without exception of any material. Coulombic efficiencies of borides after initial discharge were calculated as 42.9, 59.8, 57.1, and 68.5% for MnB, MoB, FeB, and VB, respectively. The efficiency of VB showed notably higher than other samples while the colombic efficiency of MnB not even reached 50%. $MnBO_3$ and YBO_3 showed colombic efficiency of 56.4 and 50.6%, respectively. Rate capability was also tested via charge and discharge of samples 5 times at 20, 50, and 100 mA/g. The effect of rate change during galvanostatic charge and discharge was noticeably small. There were no large capacity decreases observed with an increase in current density.

The average specific capacity of five cycles at 100 mA/g current density was noted as 247.63 mAh/g for MoB which is the highest measured capacity of all boron-based samples that are synthesized during this study.

The stability of samples was tested by cycling them for fifty cycles at 20 mA/g. decrease in capacity throughout the cyclic process continued. The capacity retention of MoB, VB, MnB, and FeB were calculated as 73.55, 85.37, 54.99, and 70.01%, respectively. VB has remarkable capacity retention more than 10 percent higher than the closest boride. $MnBO_3$ is the material that had the lowest capacity retention not only among borates but also lower than any boride that is tested during this study. The capacity retention of 41.23% was noted. On the other hand, 84.48% was the highest capacity retention which belongs to YBO_3 achieved during this study. However, this retention did not consider as important as VB since the specific capacity of YBO_3 was drastically low.

For further analysis CV analysis of samples at 0.02, 0.05, and 0.08 mV/ scan rate was made. This analysis aimed to investigate any reactions that occur during lithiation and delithiation of cells. At the initial cycle, it was noted that boron-based anode materials cause an SEI formation with electrolyte decomposition around 0.74 V. SEI formation and irreversible reaction that occurs at certain samples explain the reasoning for huge capacity drops after the first cycles of galvanostatic charge and discharge of borides as well as borates.

REFERENCES

1. Goodenough, J. B. Evolution of strategies for modern rechargeable batteries. *Acc. Chem. Res.* **46**, 1053–1061 (2013).

2. Li, M., Lu, J., Chen, Z. & Amine, K. 30 Years of Lithium-Ion Batteries. *Adv. Mater.* **30**, (2018).

3. Nitta, N., Wu, F., Lee, J. T. & Yushin, G. Li-ion battery materials: Present and future. *Mater. Today* **18**, 252–264 (2015).

4. Xie, Y., Jin, Y. & Xiang, L. Understanding Mn-based intercalation cathodes from thermodynamics and kinetics. *Crystals* **7**, (2017).

5. Padhi, A. K., Nanjundaswamy, K. S. & Goodenough, J. B. Phospho-olivines as Positive-Electrode Materials for Rechargeable Lithium Batteries. *J. Electrochem. Soc.* **144**, 1188–1194 (1997).

6. Guerfi, A. *et al.* Temperature Effect on LiFePO4 Cathode Performance. *ECS Trans.* **3**, 3–17 (2007).

7. Molenda, J. & Molenda, M. Composite Cathode Material for Li-Ion Batteries Based on LiFePO4 System. *Met. Ceram. Polym. Compos. Var.*

Uses (2011) doi:10.5772/21635.

8. Soc, 小槻勉 - J. Electrochem. & 1990, undefined. 資源と素材: 資源・素材学会誌: journal of the Mining and Materials Processing Institute of Japan 117 (6), 479-483, 2001-06-25. *ci.nii.ac.jp*.

9. Delmas, C., Saadoune, I. & Rougier, A. The cycling properties of the LixNi1-yCoyO2 electrode. *J. Power Sources* **44**, 595–602 (1993).

10. Yabuuchi, N. & Ohzuku, T. Novel lithium insertion material of LiCo1/3Ni1/3Mn1/3O2 for advanced lithium-ion batteries. *J. Power Sources* **119**–**121**, 171–174 (2003).

11. Julien, C. M. & Mauger, A. Lithium-Ion Batteries. (2020).

12. Wu, J., Cao, Y., Zhao, H., Mao, J. & Guo, Z. The critical role of carbon in marrying silicon and graphite anodes for high-energy lithium-ion batteries. *Carbon Energy* **1**, 57–76 (2019).

13. Chemistry Roadmap - Battery Design. https://www.batterydesign.net/chemistry-roadmap/.

14. A.K. Padhi, K.S. Nanjundaswamy, J.B. Goodenough,... - Google Akademik.

https://scholar.google.com/scholar?hl=tr&as_sdt=0%2C5&q=A.K.+Padhi%2C+K.S.+Nanjundaswamy%2C+J.B.++Goodenough%2C+J.+Electrochem.+Soc.+144+%281997%29+1188.++%5B5%5D+N.+Ravet%2C+Y.+Chouinard%2C+J.F.+Magnan%2C+S.+Besner%2C++M.+Gauthier%2C+M.+Armand%2C+J.+Power+Sources+97%2F98++%282001%29+503.&btnG=.

15. Chung, S., Bloking, J., materials, Y. C.-N. & 2002, undefined. Electronically conductive phospho-olivines as lithium storage electrodes. *nature.com*.

16. Kang, B., Nature, G. C.- & 2009, undefined. Battery materials for ultrafast charging and discharging. *nature.com*.

17. Recham, N. *et al.* Ionothermal synthesis of tailor-made LiFePO4 powders for li-ion battery applications. *Chem. Mater.* **21**, 1096–1107 (2009).

18. Yamada, A., Iwane, N., Harada, Y., … S. N.-A. & 2010, undefined. Lithium iron borates as high-capacity battery electrodes. *Wiley Online Libr.* **22**, 3583–3587 (2010).

19. Zhang, B., Zhu, Y., Yu, W. J., Zhang, J. F. & An, C. Facile synthesis of carbon-encapsulated LiMnBO3 composite by the sol-gel method as a lithium-ion battery cathode material. *J. Alloys Compd.* **704**, 343–347 (2017).

20. Afyon, S., Kundu, D., Krumeich, F. & Nesper, R. Nano LiMnBO3, a high-capacity cathode material for Li-ion batteries. *J. Power Sources* **224**, 145–151 (2013).

21. Kim, J. C., Seo, D. H. & Ceder, G. Theoretical capacity achieved in a LiMn 0.5 Fe 0.4 Mg 0.1 BO 3 cathode by using topological disorder. *Energy Environ. Sci.* **8**, 1790–1798 (2015).

22. Goodenough, J. B. & Kim, Y. Challenges for rechargeable Li batteries. *Chem. Mater.* **22**, 587–603 (2010).

23. Ibarra-Palos, A. *et al.* Electrochemical reactions of iron borates with lithium: Electrochemical and in situ Mössbauer and X-ray absorption studies. *Chem. Mater.* **14**, 1166–1173 (2002).

24. Yu, M. *et al.* 3D Hollow Porous Spherical Architecture Packed by Iron-Borate Amorphous Nanoparticles as High-Performance Anode for Lithium-Ion Batteries. *ACS Appl. Mater. Interfaces* **11**, 25254–25263 (2019).

25. Zeng, X. *et al.* Synthesis, structure, and electrochemical performance of V3BO6 nanocomposite: A new vanadium borate as high-rate anode for Li-ion batteries. *Electrochim. Acta* **335**, 135661 (2020).

26. Kim, D. Y., Song, M. S., Eom, J. Y. & Kwon, H. S. Synthesis of VBO 3-

carbon composite by ball-milling and microwave heating and its electrochemical properties as negative electrode material of lithium ion batteries. *J. Alloys Compd.* **542**, 132–135 (2012).

27. Wu, D., Kuang, Q., Zhao, Y., Liu, S. & Fan, Q. Sol-gel synthesized carbon-coated vanadium borate as anode material for rechargeable Li and Na batteries. *J. Alloys Compd.* **732**, 506–510 (2018).

28. Dong, W. *et al.* Boron Embedded in Metal Iron Matrix as a Novel Anode Material of Excellent Performance. *Adv. Mater.* **30**, 1801409 (2018).

29. Guo, Z., Zhou, J. & Sun, Z. New two-dimensional transition metal borides for Li ion batteries and electrocatalysis. *J. Mater. Chem. A* **5**, 23530–23535 (2017).

30. Gao, S. *et al.* Two dimension transition metal boride Y2B2 as a promising anode in Li-ion and Na-ion batteries. *Comput. Mater. Sci.* **200**, 110776 (2021).

31. Xiong, W. *et al.* Fluorine-free prepared two-dimensional molybdenum boride (MBene) as a promising anode for lithium-ion batteries with superior electrochemical performance. *Chem. Eng. J.* **446**, 137466 (2022).

32. Netz, A., Huggins, R. A. & Weppner, W. Investigations of a number of

alternative negative electrode materials for use in Lithium cells. *Ionics (Kiel).* **7**, 433–439 (2001).

33. Liu, Y. *et al.* Structure and electrochemical behaviors of a series of Co–B alloys. *Electrochim. Acta* **53**, 2265–2271 (2008).

34. Wang, D. *et al.* Cobalt-boron nanoparticles anchored on graphene as anode of lithium ion batteries. *Chem. Eng. J.* **360**, 271–279 (2019).

35. Zoli, L., Galizia, P., Silvestroni, L. & Sciti, D. Synthesis of group IV and V metal diboride nanocrystals via borothermal reduction with sodium borohydride. *J. Am. Ceram. Soc.* **101**, 2627–2637 (2018).

36. Wang, Y. D., Ai, X. P. & Yang, H. X. Electrochemical hydrogen storage behaviors of ultrafine amorphous Co-B alloy particles. *Chem. Mater.* **16**, 5194–5197 (2004).

37. Zoli, L., Galizia, P., Silvestroni, L. & Sciti, D. Synthesis of group IV and V metal diboride nanocrystals via borothermal reduction with sodium borohydride. *J. Am. Ceram. Soc.* **101**, 2627–2637 (2018).

38. Yang, Y. *et al.* Iron Phosphide Confined in Carbon Nanofibers as a Free-Standing Flexible Anode for High-Performance Lithium-Ion Batteries. *Cite This ACS Appl. Mater. Interfaces* **13**, 34083 (2021).

39. Xu, Q. T., Li, J. C., Xue, H. G. & Guo, S. P. Effective combination of FeS2 microspheres and Fe3S4 microcubes with rGO as anode material for high-capacity and long-cycle lithium-ion batteries. *J. Power Sources* **396**, 675–682 (2018).

40. Sun, X. *et al.* Amorphous vanadium oxide coating on graphene by atomic layer deposition for stable high energy lithium ion anodes † ChemComm. *Chem. Commun* **50**, 10703–10706 (2014).

41. Ni, S., Liu, J., Chao, D. & Mai, L. Vanadate-Based Materials for Li-Ion Batteries: The Search for Anodes for Practical Applications. *Adv. Energy Mater.* **9**, (2019).

42. Yi, H. *et al.* The manganese oxyborate Mn3(BO3)2 as a high-performance anode for lithium-ion batteries. *Solid State Ionics* **380**, 1–7 (2022).

43. Rui, K., Wen, Z., Lu, Y., Jin, J. & Shen, C. One-Step solvothermal synthesis of nanostructured manganese fluoride as an anode for rechargeable lithium-ion batteries and insights into the conversion mechanism. *Adv. Energy Mater.* **5**, (2015).

44. Zhang, Y. *et al.* Layered Perovskite Lithium Yttrium Titanate as a Low-Potential and Ultrahigh-Rate Anode for Lithium-Ion Batteries. *Adv. Energy Mater.* (2022) doi:10.1002/AENM.202200922.